CHEMISTRY
A EUROPEAN JOURNAL

DOI: 10.1002/chem.201000554

Reactivity of the Latent 12-Electron Fragment $[Rh(P\textit{i}Bu_3)_2]^+$ with Aryl Bromides: Aryl–Br and Phosphine Ligand C–H Activation

Nell S. Townsend,[a] Adrian B. Chaplin,[a] M. Abu Naser,[b] Amber L. Thompson,[a] Nicholas H. Rees,[a] Stuart A. Macgregor,*[b] and Andrew S. Weller*[a]

Abstract: Oxidative addition of aryl bromides to 12-electron $[Rh(P\textit{i}Bu_3)_2][BAr^F_4]$ ($Ar^F = 3,5\text{-}(CF_3)_2C_6H_3$) forms a variety of products. With *p*-tolyl bromides, Rh^{III} dimeric complexes result $[Rh(P\textit{i}Bu_3)_2(o/p\text{-}MeC_6H_4)(\mu\text{-}Br)]_2[BAr^F_4]_2$. Similarly, reaction with *p*-ClC_6H_4Br gives $[Rh(P\textit{i}Bu_3)_2(p\text{-}ClC_6H_4)(\mu\text{-}Br)]_2[BAr^F_4]_2$. In contrast, the use of *o*-BrC_6H_4Me leads to a product in which toluene has been eliminated and an isobutyl phosphine has undergone C–H activation: $[Rh\{P\textit{i}Bu_2(CH_2CHCH_3CH_2)\}(P\textit{i}Bu_3)(\mu\text{-}Br)]_2[BAr^F_4]_2$. Trapping experiments with *ortho*-bromo anisole or *ortho*-bromo thioanisole indicate that a possible intermediate for this process is a low-coordinate Rh^{III} complex that then undergoes C–H activation. The anisole and thioanisole complexes have been isolated and their structures show OMe or SMe interactions with the metal centre alongside supporting agostic interactions, $[Rh(P\textit{i}Bu_3)_2(C_6H_4OMe)Br][BAr^F_4]$ (the solid-state structure of the 5-methyl substituted analogue is reported) and $[Rh(P\textit{i}Bu_3)_2(C_6H_4SMe)Br][BAr^F_4]$. The anisole-derived complex proceeds to give $[Rh\{P\textit{i}Bu_2(CH_2CHCH_3CH_2)\}(P\textit{i}Bu_3)(\mu\text{-}Br)]_2[BAr^F_4]_2$, whereas the thioanisole complex is unreactive. The isolation of $[Rh(P\textit{i}Bu_3)_2(C_6H_4OMe)Br][BAr^F_4]$ and its onward reactivity to give the products of C–H activation and aryl elimination suggest that it is implicated on the pathway of a σ-bond metathesis reaction, a hypothesis strengthened by DFT calculations. Calculations also suggest that C–H bond cleavage through phosphine-assisted deprotonation of a non-agostic bond is also competitive, although the subsequent protonation of the aryl ligand is too high in energy to account for product formation. C–H activation through oxidative addition is also ruled out on the basis of these calculations. These new complexes have been characterised by solution NMR/ESIMS techniques and in the solid-state by X-ray crystallography.

Keywords: agostic interactions · C–H activation · density functional calculations · transition metals · X-ray diffraction

Introduction

The oxidative addition of aryl halides to late-transition-metal centres, especially Pd^0, is central to metal-mediated transformations such as C–C and C–N coupling reactions.[1] Studies show that $[Pd(PR_3)_2]$ and related N-heterocyclic carbene-ligated fragments react with aryl halides by mechanisms that depend on the identity of the haloarene. In some cases one-coordinate Pd^0, formally 12-electron complexes, are identified as the reactive species, which undergo oxidative addition with aryl halides.[2,3] The number of examples of well-characterised group 9 species capable of undergoing oxidative addition with aryl halides is relatively small, but growing.[4,5] The study of such species and their onward reactivity is important in terms of future efforts to develop the use of group 9 species in C–C and C–N coupling reactions. Recently, the use of rhodium and iridium complexes have been reported in C–C and C–N cross-coupling reactions,[6]

[a] N. S. Townsend, Dr. A. B. Chaplin, Dr. A. L. Thompson, Dr. N. H. Rees, Prof. A. S. Weller
Department of Chemistry
Inorganic Chemistry Laboratory, University of Oxford
South Parks Road, Oxford, OX1 3QR (UK)
Fax: (+44) 1865 272690
E-mail: andrew.weller@chem.ox.ac.uk

[b] Dr. M. A. Naser, Prof. S. A. Macgregor
Heriot-Watt University
Riccarton, Edinburgh, EH14 4AS (UK)
School of Engineering and Physical Sciences
Fax: (+44) 131 451 3180
E-mail: S.A.Macgregor@hw.ac.uk

Supporting information for this article is available on the WWW under http://dx.doi.org/10.1002/chem.201000554.

and these reactions are suggested to proceed through low-coordinate, electronically unsaturated intermediates that undergo aryl halide oxidative addition. Aryl halide oxidative additions are also interesting from the standpoint of dechlorination reactions of polychloroaromatics.[7] More generally, the study of the onward reactivity of well-characterised low-coordinate late-transition-metal complexes is of relevance to many catalytic processes that rely on the generation of such species.

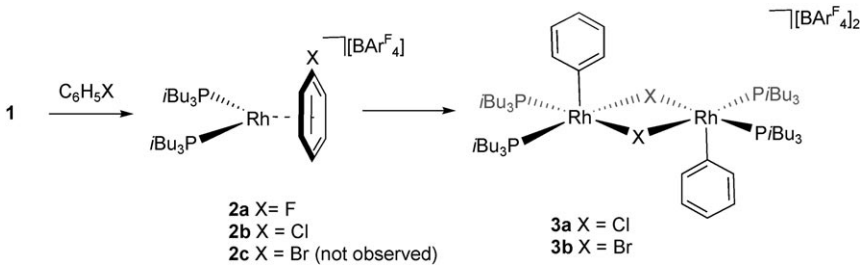

Scheme 2. Formation of an intermediate arene complex and subsequent oxidative cleavage.

We have previously reported the synthesis of $[Rh(P iBu_3)_2(H)_2][BAr^F_4]$ ($Ar^F = 3,5\text{-}(CF_3)_2C_6H_3$), which has a cationic Rh^{III} centre with two supporting agostic interactions from the tris(isobutyl)phosphine ligands (Scheme 1).[8] It is related to $P iPr_3$ and PCy_3 analogues[9] and Ir–dihydride bis(phosphine) or bis(N-heterocyclic) carbene species.[10,11] Placing this dihydride complex under vacuum or addition of a hydrogen acceptor (*tert*-butylethene) results in the quantitative formation of a Rh^I species that we have formulated as $[Rh(P iBu_3)_2][BAr^F_4]$ (**1**),[12] which is formally a 12-electron metal complex, although there are no doubt supporting agostic C–H interactions from the phosphine alkyl groups.[10,11,13] NMR spectroscopy and trapping experiments support this formulation, with addition of C_6H_5F resulting in the formation of the arene adduct $[Rh(\eta^6\text{-}C_6H_5F)(P iBu_3)_2][BAr^F_4]$ (**2a**). Complex **1** also takes part in oxidative addition reactions. For example, it catalyses the dehydrocoupling of amine boranes,[13,14] which are suggested to proceed through B–H oxidative addition,[13,15] whereas addition of C_6H_5X (X = Cl, Br) to **1** results in 16-electron dimeric complexes **3a** and **3b** that are the product of oxidative cleavage of the Ar–X bond (Scheme 2).[8] For X = Cl an intermediate was both spectroscopically[8] and crystallographically[16] identified as an η^6-arene adduct, **2b**. Adducts that are η-bound have previously been implicated in a number of oxidative cleavage reactions of aryl halides at low-valent transition-metal centres.[3,17]

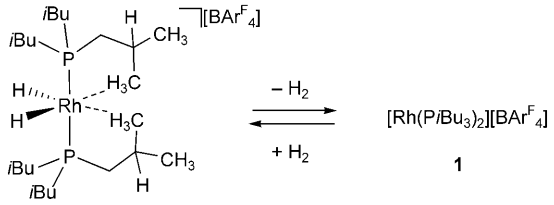

Scheme 1. Synthesis of **1** from $[Rh(P iBu_3)_2(H)_2][BAr^F_4]$.

Herein, we extend the scope of this reactivity to include aryl bromides of differing steric and electronic profiles. This leads to the products of oxidative cleavage of the aryl–halide bond as well as, unexpectedly, C–H activation of the phosphine, for which we also present a computational investigation.

Results and Discussion

Oxidative addition of aryl bromides: Addition of *p*-ClC_6H_4Br, *p*-MeC_6H_4Br and *m*-MeC_6H_4Br to C_6H_5F solutions of **2a** results in the precipitation of the new dimeric dications $[Rh(P iBu_3)_2(p\text{-}ClC_6H_4)(\mu\text{-}Br)]_2[BAr^F_4]_2$ (**4**), $[Rh(P iBu_3)_2(p\text{-}MeC_6H_4)(\mu\text{-}Br)]_2[BAr^F_4]_2$ (**5**) and $[Rh(P iBu_3)_2(m\text{-}MeC_6H_4)(\mu\text{-}Br)]_2[BAr^F_4]_2$ (**6**) in reasonable isolated yields, which are the products of oxidative addition of the corresponding aryl bromide (Scheme 3). No intermediate species were observed, unlike in the case of addition of ClC_6H_5 (with the stronger Ar–Cl bond) in which an intermediate η^6-π complex (**2b**) was observed prior to oxidative cleavage of the C–Cl bond.[8] All are formulated as dimeric $[Rh_2]^{2+}$ salts. The solid-state structures for the cationic part of the salts are shown in Figure 1, with selected bond lengths and angles in Table 1. These dimers are closely related to those reported by Budzelaar, which come from addition of aryl halides to the low-coordinate Rh^I complex $[\{(Me_2C_6H_3)NCMeCHCMeN(Me_2C_6H_3)\}Rh(coe)]$ (coe = cy-

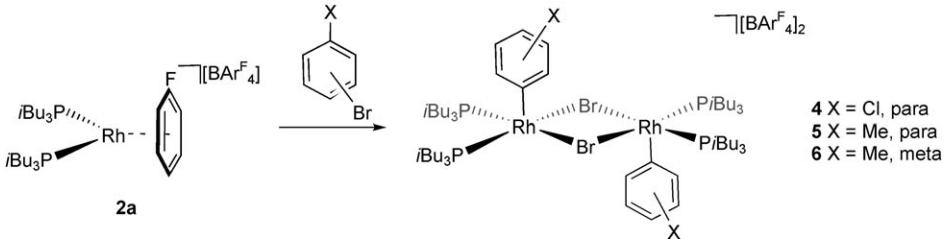

Scheme 3. Synthesis of dimeric salts **4**–**6**.

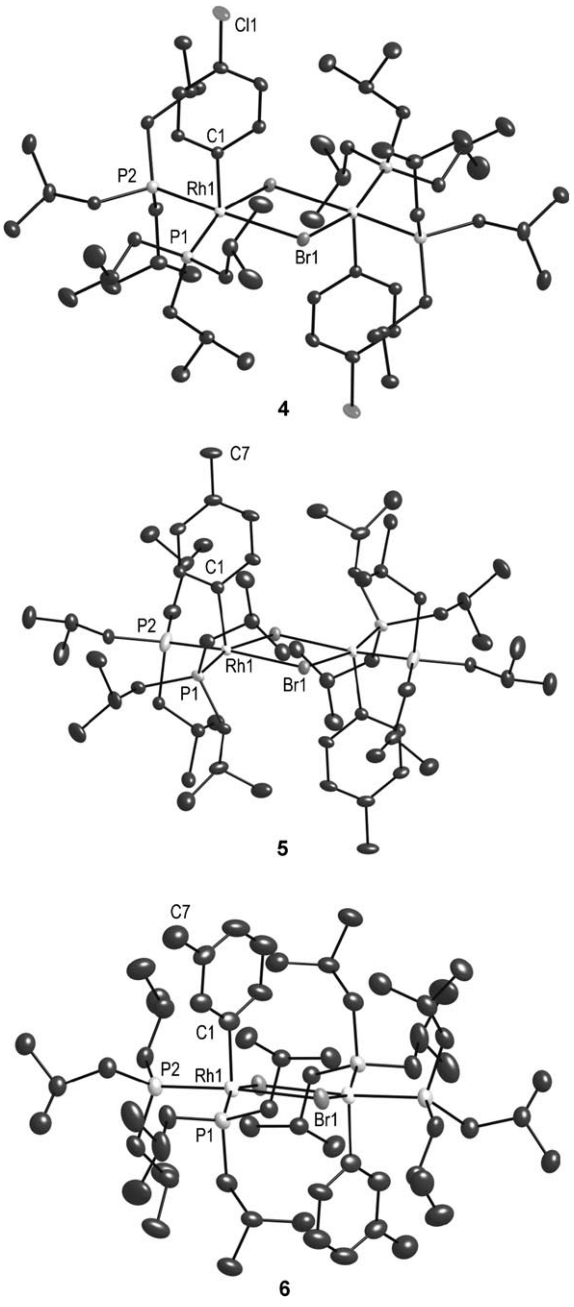

Figure 1. Solid-state structure of the cationic portions of complexes **4**, **5** and **6**. Thermal ellipsoids are shown at the 30% probability level. All are centrosymmetric dimers and are generated by the appropriate symmetry operations. Only one of the crystallographically independent cations in the unit cell is shown for **5**. See Table 1 for selected bond lengths and angles. Hydrogen atoms and minor disordered components are omitted for clarity.

clooctene).[5] It is also well-established that halide-bridged dimer species arise from oxidative addition of aryl halides to $[Pd(L)_2]$.[18]

In the solid-state complexes, **4**, **5** and **6** crystallise as centrosymmetric dimers, and for **5** there are also two independent molecules in the unit cell, which do not differ significantly in their structural metrics. All three dimers have 16-electron Rh^{III}, five-coordinate pseudo-square-based pyramidal centres with an apical aryl group *trans* to a vacant site, as might be expected.[19] The phosphines are situated *cis* to one another. The long Rh···Rh distances of approximately 4 Å rule out metal–metal bonding. The Rh–C_{aryl} lengths are similar to those reported in **3a** and **3b**.[8] The aryl groups are orientated mutually *anti* and lie parallel to the Rh···Rh vector, and this orientation is presumably enforced by steric constraints from the phosphine ligands as demonstrated by the space-filling diagram of **6** (Figure 2). This orientation also means that the *cis* phosphines and the *cis* bromides sit in a square plane. As demonstrated later, bulky aryl groups that disrupt this motif do not allow the formation of the dimer, and the resulting low-coordinate metal fragment undergoes further reaction (C–H activation of the alkyl phosphine group). The vacant sites on each Rh centre in these dimers could be completed by an agostic interaction[20] from an isobutyl group, but the closest Rh···C distances are all greater than 3.1 Å, indicating that any interactions are weak at best[21] (compare with [RhClH(I*t*Bu)(I*t*Bu')], I*t*Bu = *N*,*N*-di(*tert*-butyl)imidazol-2-ylidene, which has a strong agostic interaction, Rh···C 2.704 Å).[22] The presence of a vacant site and the proximity of an alkyl group does not necessarily mean that an agostic interaction will always be present because other competing factors (electronic and steric) play a part,[23, 24] especially if a strong *trans*-influence ligand is pres-

Table 1. Comparison of selected bond lengths [Å] and angles [°] for complexes **4**, **5**, **6** and **7**.

	4	**5**	**6**	**7**
Rh1–C1	2.012(3)	2.018(7), 2.018(8)	2.022(4)	–
Rh1–C3	–	–	–	2.086(4)
Rh1–P1	2.3332(8)	2.318(2), 2.312(2)	2.291(1)	2.2778(8)
Rh1–P2	2.3186(8)	2.311(2), 2.309(2)	2.294(1)	2.2913(8)
Rh–Br1	2.5765(4)	2.5736(8), 2.5937(10)	2.5890(5)	2.5731(4)
Rh–Br#1	2.5896(4)	2.5974(7), 2.6066(9)	2.5851(5)	2.5839(4)
P1-Rh1-P2	101.45(3)	105.07(8), 102.78(9)	99.55(4)	94.13(3)
C1-Rh1-P1	89.20(8)	88.9(2), 88.9(2)	97.1(1)	–
C3-Rh1-P1	–	–	–	94.1(1)
C1-Rh1-P2	93.25(8)	90.0(2), 93.1(2)	91.2(1)	–
C3-Rh1-P2	–	–	–	83.37(1)
Rh#1-Rh1-C1	103.02(8)	103.7(2), 103.4(2)	103.2(2)	–

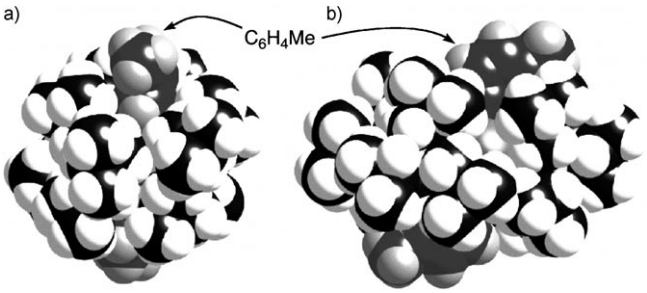

Figure 2. Space-filling diagram of complex **6** with the aryl groups highlighted. a) Perspective parallel to the Rh···Rh axis and b) perspective orthogonal to the Rh···Rh axis.

ent.[25] Crystallographically characterised complexes that have agostic isobutyl phosphine ligands show slightly shorter M···C distances than in **4**–**6**, for example, $[Rh(P\mathit{i}Bu_3)_2(H)_2][BAr^F{}_4]$ (ca. 2.9 Å)[8] and $[Mo(CO)(\mathit{i}Bu_2PC_2H_4P\mathit{i}Bu_2)_2]$ (ca. 3.0 Å).[26] The dimeric, bis-agostic motif has been reported previously for a series of neutral halide-bridged complexes $[Ru_2H_nX_{4-n}(P\mathit{i}Pr_3)_4]$ (X = F, Cl).[23]

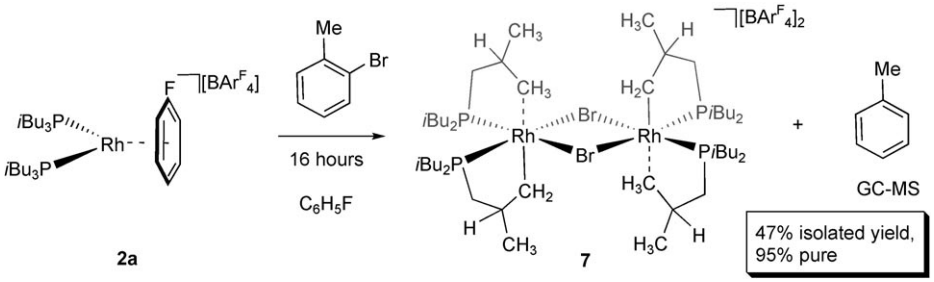

Scheme 4. Synthesis of complex **7**.

In solution, NMR spectroscopy shows one ^{31}P environment with coupling to ^{103}Rh (with $J(Rh,P) \approx 139$ Hz) for all the new complexes **4**–**6**. The ^1H NMR spectra show two diastereotopic methyl environments for the *i*Bu groups in addition to aryl signals. Although these data do not discriminate against monomeric complexes such as $[Rh(P\mathit{i}Bu_3)_2(aryl)Br]^+$, in solution the high reactivity of such a 14-electron species (see below) coupled with the fact that the compounds show, at best, only moderate solubility in suitable common solvents (CD_2Cl_2 and C_6H_5F) suggests that the dimeric dicationic formulation is retained in solution. The low solubility in these solvents also means that low-temperature NMR spectra were not obtained precluding the investigation of any potential agostic interactions in solution. ESIMS shows monotonic isotopomer progression and the correct isotope pattern, indicating that the dimers break up to monomers in the gas phase under ESI conditions.

Complex **4** does not undergo further reaction, that is, Ar–Cl activation, when more **2** is added even though we have established that oxidative addition of free chlorobenzene happens readily with **2**.[8] This is no doubt due to the incoming metal fragment being unable to form a precursor π-complex necessary for cleavage of the Ar–Cl bond (Figure 2). The isolation of **4** as the product of Ar–Br oxidative addition indicates the kinetic preference for Ar–Br activation over Ar–Cl.

Reactivity with bulky aryl bromides: Addition of *o*-MeC_6H_4Br to **2** did not result in the isolation of the direct product of Ar–Br oxidative addition. Instead a dimeric species was isolated as the final product, which contains no aryl group and has undergone C–H activation of one of the alkyl phosphine groups to give $[Rh\{P\mathit{i}Bu_2(CH_2CHCH_3CH_2)\}(P\mathit{i}Bu_3)(\mu\text{-}Br)]_2[BAr^F{}_4]_2$ (**7**; Scheme 4). Complex **7** was isolated by crystallisation and obtained in approximately 50% yield as a 95% pure material and was contaminated with small amounts of unidentified phosphine-containing materials. Monitoring the reaction by NMR spectroscopy ($^{31}P\{^1H\}$) indicated conversion higher than this (~80%) alongside the production of unidentified materials. Analysis of the reaction mixture by GC–MS also showed the formation of toluene as a co-product, suggesting that addition of the Ar–Br bond to the metal is followed eventually by the elimination of ArH. We return to the details of this transformation later.

In the solid state **7** crystallises as a centrosymmetric dicationic dimer in which each Rh^{III} centre is a pseudo-square-based pyramid, similar to that observed for **4**, **5** and **6** (Figure 3 and Table 1). This structural similarity extends to the $\{RhP_2Br_2\}$ core: the Rh–C covalent bond, this time

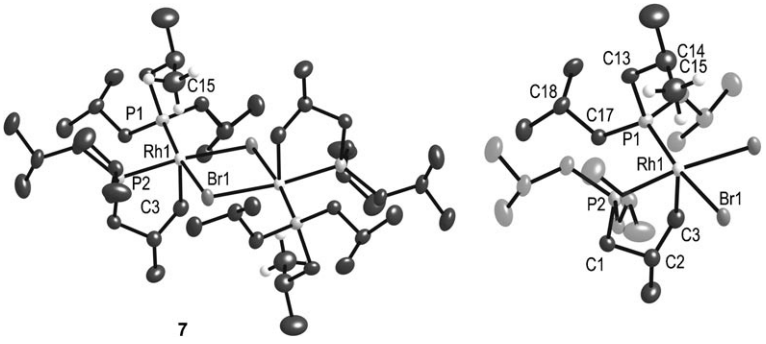

Figure 3. Left: Solid-state structure of the cationic portion of complex **7**. Thermal ellipsoids are shown at the 50% probability level. Right: Crystallographically unique portion of the dimer highlighting selected *i*Bu groups. Both bridging bromide atoms have been shown for clarity. Selected bond lengths and angles are given in Table 1. Hydrogen atoms, except for those associated with C15 (calculated) and minor disordered components, have been omitted for clarity.

coming from a C–H activated *i*Bu phosphine substituent that lies *trans* to the vacant site, and a weak at best[21] agostic interaction (Rh···C15 3.049 Å) between an alkyl phosphine CH_3 group and the Rh centre. The hydrogen atoms associated with the agostic CH_3 groups were not located in the final difference map and were placed in calculated positions. The two cyclometallated alkyl groups in the dimer lie

anti to each other and are related by an inversion centre. The P-C-C angle associated with the metallated alkyl group [Rh1-P2-C1, 102.9(1)°] is more acute than that of the agostic interaction [Rh1-P1-C13, 106.3(1)°], although both are smaller than those of the other, non-interacting alkyl groups [114–119°].

Although the room-temperature NMR spectra of recrystallised **7** are rather broad, and poor solubility in suitable solvents precluded a low-temperature study, in solution the ^{1}H NMR spectrum shows evidence for two isomers by the observation of two sets of resonances centred at $\delta = 4.37$ (2H) and 3.20 ppm (2H) that are further split within themselves in an approximate 1:2 ratio. The downfield shift of these compared with the free ligand is consistent with a cyclometallated alkyl group.[22,27] Although we have not been able to unambiguously assign these resonances to specific CH_2 groups, it is most likely that they belong to the diastereotopic protons on either C1 or C3 (Figure 3) because they are absent in the spectra of **4**, **5** and **6**. Two isomeric species in an approximate 1:2 ratio are also observed in the $^{31}P\{^1H\}$ NMR spectrum as a set of doublet of doublets showing *cis* ^{31}P–^{31}P coupling, as well as coupling to the Rh^{III} centre ($J(P,P) = 28$, $J(Rh,P) \approx 142$ Hz). ESIMS shows a single, dicationic organometallic species consistent with the solid-state structure (m/z: calcd: 586.1848; found: 586.1851; $z = 2$) adding support to these two complexes being simple isomers. Four sets of probable isomers in **7** can be envisaged in which the cyclometallated (or agostic) groups are either *syn* or *anti* with respect to planes perpendicular and parallel to the Rh_2Br_2 plane. The solid-state structure shows one of these: *anti*/*anti*. All isomers would have two ^{31}P environments. Monitoring the reaction between **2** and *o*-MeC_6H_4Br by $^{31}P\{^1H\}$ NMR spectroscopy shows that after 16 h four separate isomeric complexes can be observed, which eventually resolve into two after standing for four days, that is, a similar timescale to recrystallisation. This suggests a slow (laboratory timescale) equilibration. This monitoring also reveals a species that grows in intensity early in the reaction and then gradually disappears, which is consistent with the behaviour of an intermediate ($\delta = 60.8$ ppm; $J(Rh,P) = 160$ Hz). We tentatively assign this to be the monometallic species $[Rh(P\mathit{i}Bu_3)_2Br(\mathit{o}\text{-}C_6H_4Me)][BAr^F{}_4]$ (**A**; Scheme 5) on the basis of the similarity of ^{31}P chemical shift to that of monometallic **8** (see below). Reaction with mesityl bromide also afforded **7** as the organometallic product,[28] but the reaction was not as clean.

C–H activation of alkyl phosphines to low-valent metal centres is well established, especially with *t*Bu and *i*Pr groups on phosphines[27,29,30] or N-heterocyclic carbenes.[10,22,31] We are not aware of a well-defined example of C–H activation of isobutyl phosphines although C–H activation of *neo*-pentyl phosphines has been reported.[32] The mechanism of the process occurring here to form **7** is discussed in the next section.

Intermediates in the C–H activation process: The C–H activation that occurs to afford **7** is particularly noteworthy because it appears to take place at a Rh^{III} centre formed after Ar–Br oxidative addition to the precursor Rh^I complex **2**. C–H activation at a metal centre can occur by oxidative addition or by σ-bond metathesis,[33,34] with the continuum of transition states in between making definitive categorisation sometimes difficult.[35,36,37] A closely related σ-CAM (CAM = complex assisted metathesis) mechanism has recently been suggested in which a σ-bond metathesis transformation occurs with the additional formation of a stable σ-adduct before and after the actual metathesis.[34,36] Alternatively, electrophilically induced deprotonation of a σ-bound intermediate is possible in which a base (internal or external) deprotonates an activated C–H bond that is coordinated through a sigma interaction with the metal.[38,39] A recent twist in this pathway is the demonstration that a geminal C–H bond that is not involved in an agostic interaction can be deprotonated.[40] C–H activation at a Rh^{III} centre is relatively rare,[22,41] and it is unlikely to occur by oxidative addition, which would involve a Rh^V intermediate.[42] This can be compared to C–H activation at Ir^{III} for which the +5 oxidation state is more accessible. For example $[Cp^*Ir(PMe_3)H(ClCH_2Cl)][BAr^F{}_4]$ ($Cp^* = \eta^5\text{-}C_5Me_5$) is well-known to undergo C–H activation chemistry with alkanes[43] through an Ir^V intermediate,[44] whereas $[Cp^*Rh(PMe_3)H(ClCH_2Cl)][BAr^F{}_4]$ does not react with alkanes.[45] Likewise addition of H_2 to $[Cp^*Rh(PMe_3)H(ClCH_2Cl)][BAr^F{}_4]$ gives a Rh^{III} dihydrogen/dihydride complex $[Cp^*Rh(PMe_3)H(H_2)][BAr^F{}_4]$,[46] whereas the Ir congener is a Ir^V trihydride $[Cp^*Ir(PMe_3)H_3][BAr^F{}_4]$, albeit prepared by a different route.[47]

The observation by GC–MS of toluene as a co-product in the formation of **7** from **2a** and *o*-MeC_6H_4Br suggests oxidative addition of the Ar–Br bond as an early step in the reaction. This would give a cationic Rh^{III}-aryl species that then undergoes C–H activation to ultimately generate toluene and the cyclometallated phosphine complex. The fact that local steric bulk *ortho* to the Ar–Br bond promotes this reaction suggests that the stable dimeric motifs observed for complexes **4**–**6** are not formed, but instead a reactive monometallic 14-electron intermediate **A** is generated (Scheme 5) for which we have spectroscopic evidence (see above). Inspection of the space-filling diagram

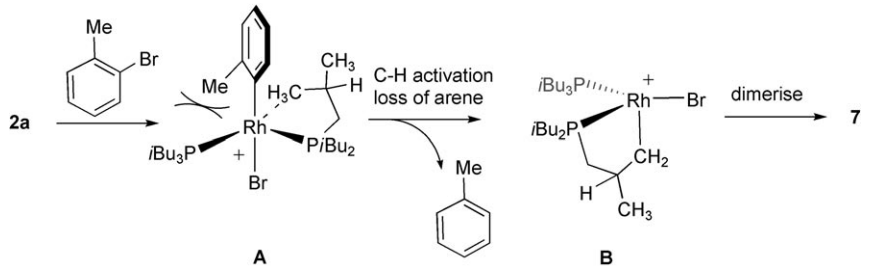

Scheme 5. Postulated mechanism for the formation of **7** from **2a** and *ortho*-bromotoluene.

of **6** (Figure 2) shows that substitution in the *ortho* position would not allow the close approach of two monomeric $\{Rh(P\mathit{i}Bu_3)_2(aryl)Br\}^+$ fragments, disfavouring dimer formation in favour of intermediate **A**. This intermediate could then proceed (by some mechanism, see below) to C–H activate and lose toluene to afford **B** (Scheme 5). **B** would likely dimerise to give the observed species **7**. To probe this mechanism, we attempted to trap out low-coordinate **A** by use of a coordinating functional group, OMe or SMe, on the arene.

Addition of *ortho*-bromo anisole to **2a** gave an immediate and clean reaction to afford the particularly air- and temperature-sensitive, dark-red complex $[Rh(P\mathit{i}Bu_3)_2(C_6H_4\dot{O}Me)Br][BAr^F{}_4]$ (**8a**) in quantitative yield (by NMR spectroscopy), which was characterised in situ by NMR spectroscopy and ESIMS. **8a** evolves over one week to give complex **7** and anisole (by GC–MS, Scheme 6). This reaction is not clean, with **7** observed in approximately 80% yield alongside other unidentified decomposition products. Nevertheless, the observation of **7** as the major final product points to **8a** being an observed intermediate in the overall C–Br oxidative addition/C–H activation reaction of **2a** with *ortho*-bromo anisole. Despite repeated attempts, isolated crystalline material of **8a** was not forthcoming. However, placing a methyl group on the anisole in the remote *meta* position gave material that was able to be crystallised in pure form, $[Rh(P\mathit{i}Bu_3)_2(5\text{-}MeC_6H_3\text{-}2\text{-}\dot{O}Me)Br][BAr^F{}_4]$ (**8b**), and it is this that we discuss in detail. Compound **8b** also evolves to give dimer **7**. The thio analogue to **8a** was also prepared, $[Rh(P\mathit{i}Bu_3)_2(C_6H_4SMe)Br][BAr^F{}_4]$ (**9**), through the same route. This complex is more stable and does not go on to form **7** even after one week at room temperature. The solid-state structures of **8b** and **9** are shown in Figure 4 and selected bond lengths and angles are given in Table 2.

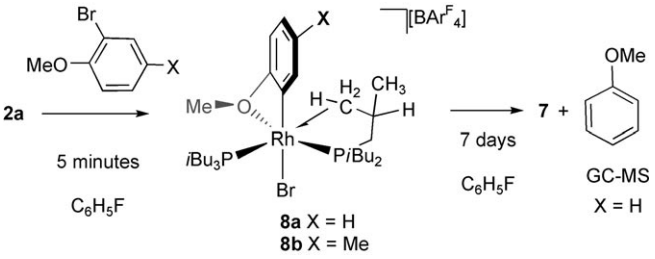

Scheme 6. Synthesis of intermediate complex **8** and its evolution into dimeric **7** and anisole.

Table 2. Comparison of selected structural metrics of **8b** and **9** (two independent molecules in the unit cell for each). Equivalent data for the computed structures of model complexes **8'** and **9'** are also given (see the text for details).

	8b	**8'**	**9**	**9'**
Rh–C1	2.01(2), 2.007(13)	2.04	2.033(4), 2.036(4)	2.05
Rh–P1	2.235(3), 2.226(4)	2.24	2.293(1), 2.2977(12)	2.30
Rh–P2	2.250(4), 2.232(13)	2.22	2.245(1), 2.2419(12)	2.22
Rh–Br1	2.500(2), 2.515(2)	2.52	2.547(1), 2.5307(6)	2.54
Rh1–O1	2.28(1), 2.282(9)	2.30	–	–
Rh1–S1	–	–	2.451(1), 2.4634(12)	2.48
Rh–C11	2.92(2), 3.023(14)	3.13	–	–
Rh–C10	–	–	3.028(5), 3.037(5)	3.11
P1-Rh1-P2	100.3(1), 99.3(1)	95.2	97.28(4), 97.89(4)	93.6
Rh1-O1-C8	128(1), 132.0(9)	129.9	–	–
Rh1-S1-C7	–	–	109.26(2), 109.1(2)	108.8
Rh1-C1-C4	157.7(7), 155.0(7)	155.2	156.3(2), 159.8(2)	160.7

In the solid-state **8b** and **9** are monomeric Rh^{III} monocations with *cis*-phosphines, an aryl–Rh bond *trans* to the halide and a coordinated (thio)ether *trans* to a phosphine to give overall pseudo-square-based pyramid geometries. Both **8b** and **9** crystallise with two independent sets of cations and anions in the unit cell, and bond lengths and angles do not differ significantly between the two in each case (Table 2). The coordination spheres are completed by a weak $Rh\cdots H_3C$ interaction from the isobutyl phosphine

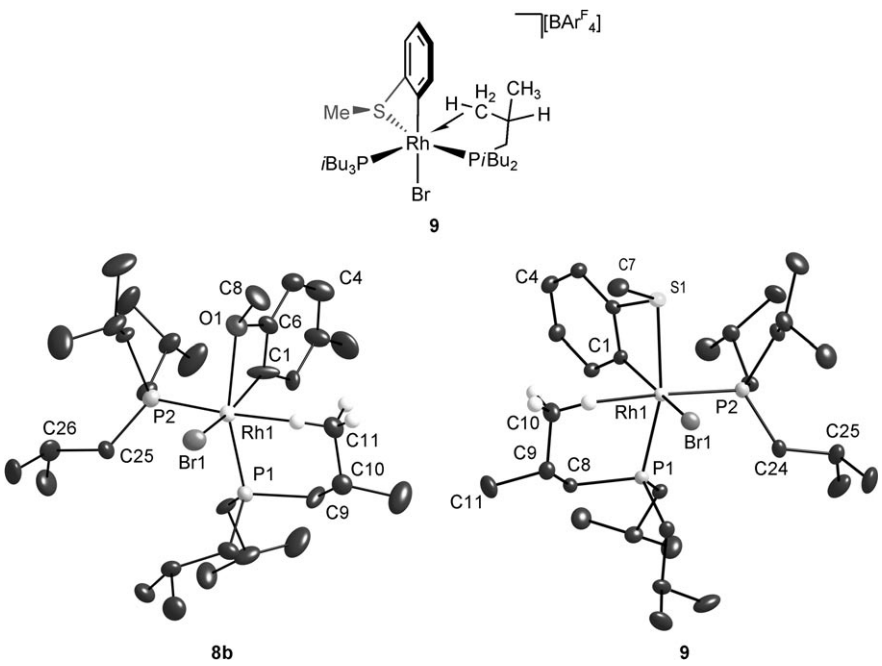

Figure 4. Solid-state structure of the cationic portions of complexes **8b** and **9**. Thermal ellipsoids are shown at the 30% probability level. Only one of the crystallographically independent salts is shown for each complex. Selected bond lengths and angles are given in Table 2. Hydrogen atoms are not shown, apart from those (calculated) associated with the agostic interaction.

(Rh···C11 = 2.92(2)/3.023(14) Å (**8b**), Rh···C10 = 3.028(5)/3.037(5) Å (**9**)). For **9** this interaction is observed in the low-temperature solution NMR spectrum. The hydrogen atoms were not located by X-ray crystallography, but DFT calculations (**8'** and **9'**, see below) support their role in weak agostic interactions with the metal centre. The corresponding Rh-P-C angles are also compressed (namely, 106–121 and 110–119° for non-interacting *i*Bu groups in **8b** and **9**, respectively). The coordination of the (thio)ether group cants the aryl group so that Rh1-C1-C4 moves away from being approximately 180° to approximately 156 and 158° for **8b** and **9**, respectively. Surprisingly, there are only a few crystallographically characterised examples of metal complexes with an *ortho*-ether-substituted aryl group, for example, $[(DMOB)_2V(TMEDA)]$ (DMOB = 2,6-dimethoxyphenyl, TMEDA = tetramethylethylenediamine).[48]

The fact that both **8b** and **9** have axial P*i*Bu$_3$ ligands *trans* to the vacant site is initially surprising because it might have been expected that the high *trans*-influence aryl ligand would occupy this site. To investigate the factors behind this isomeric preference we have performed DFT calculations on the simple model systems $[Rh(PH_3)(PH_2nPr)(C_6H_4EMe)Br]^+$ (E = O, **8'**; E = S, **9'**). This smaller model was deliberately chosen to probe electronic rather than steric effects. The computed Rh–ligand distances in these species are in good agreement with experiment (see Table 2) and evidence for agostic interactions is also seen through a computed elongation of the C–H bonds closest to the metal to approximately 1.13 Å. For both **8'** and **9'** this phosphine axial isomer is in fact only a local minimum and an alternative form with an axial aryl ligand and *cis*-phosphines is more stable by approximately 4 kcal mol^{-1}.[49] The experimental observation of the phosphine axial isomer must, therefore, be driven by steric effects associated with the P*i*Bu$_3$ ligands. Other examples in which a phosphine occupies an axial position in preference to another higher *trans*-influence ligand are known and also feature bulky phosphine substituents.[23]

Another interesting feature of **8b** and **9** is that the Rh–P1 bond length (that *trans* to O or S) is shorter by approximately 0.06 Å in the former, whereas the Rh–P2 distances in both species are the same within experimental error. This indicates a weaker *trans* Rh–O bond in **8b** compared with the Rh–S bond in **9**, a proposal supported by the solution NMR spectroscopic data (see below). These structural data are also well reproduced in the computed structures of **8'** and **9'**. One reason for the weaker Rh–O interaction may be the enhanced strain associated with the 4-membered Rh–C–C–O rings in **8b**/**8'** compared with the Rh–C–C–S rings in **9**/**9'** in which the larger S atom can interact with the Rh metal centre better. To assess this we computed the acyclic analogues of **8'** and **9'**, $[Rh(PH_3)(PH_2nPr)Ph(HOMe)Br]^+$ (**8''**) and $[Rh(PH_3)(PH_2nPr)Ph(HSMe)Br]^+$ (**9''**), and found that although the Rh–S bond did not change significantly compared to the cyclic form (Rh–S = 2.48 and 2.47 Å for **9'** and **9''**, respectively) a distinct shortening of the Rh–O bond in the MeOH species was seen (Rh–O = 2.30 and 2.23 Å for **8'** and **8''**, respectively). The smaller O atom is, therefore, less well accommodated in the four-membered ring and as a result interacts less effectively with the Rh centre. The weaker interaction has further consequences for the fluxionality of **8b** and **9**, as well as their C–H activation chemistry (see below).

In solution complexes **8b** and **9** display different time-averaged properties. Complex **8b** shows one ^{31}P environment at $\delta = 65.7$ ppm in the $^{31}P\{^1H\}$ NMR spectrum across the temperature range 298–200 K, which shows an invariant ^{103}Rh–^{31}P coupling with temperature ($J(Rh,P) = 156$ Hz), and four environments for the *i*Bu protons in the ^1H NMR spectrum at 298 K, which at 200 K resolve into five signals in the ratio 6:6:6:18:18 H relative to the BAr^F_4 protons. No high-field signals that could be assigned to an agostic interaction were observed. These data are fully consistent with a time-averaged solution structure that has C_s symmetry and equivalent phosphines, but are inconsistent with the solid-state structure. A fluxional process that makes the two phosphines equivalent, retains the Rh–P bonds and would be expected to be relatively low in energy is presented in Scheme 7.

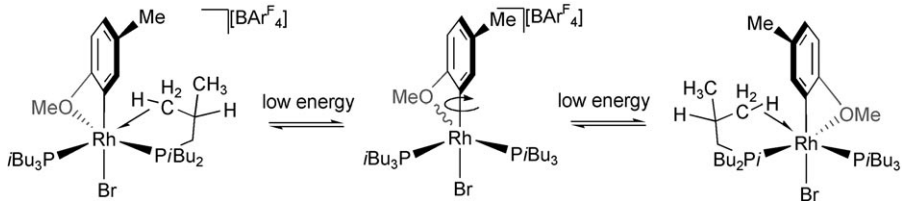

Scheme 7. Suggested low-energy fluxional pathway in **8b**.

For **9**, the room-temperature NMR spectra are different to **8b**. Two slightly broadened ^{31}P environments are observed at $\delta = 77.1$ and 34.6 ppm, which show coupling to ^{103}Rh ($J(Rh,P) \approx 150$ Hz). The ^1H resonances due to *i*Bu protons are very broad, whereas those of the aryl groups are sharp. This broadening indicates a fluxional process involving the phosphine alkyl groups that approaches the NMR timescale. The SMe group appears as a triplet ($J(P,H) = 2$ Hz) that collapses to a broad singlet on decoupling ^{31}P, demonstrating time-averaged coupling to two ^{31}P nuclei, and thus confirms metal coordination. Progressive cooling first sharpens (273 K) the phosphine signals in the $^{31}P\{^1H\}$ NMR spectrum so that they resolve as a doublet of doublets at essentially the same chemical shift as that observed at room temperature ($\delta = 77.4$ and 36.6 ppm). The ^1H NMR spectrum still shows some broad signals for the alkyl protons at 273 K, but cooling to 200 K resolves these as many sharp

signals, demonstrating that the fluxional process had been slowed down. Importantly, an integral 3H signal is now observed at $\delta = 0.145$ ppm as a broad apparent triplet (doublet of doublets), which we assign to an agostic CH_3 group on the basis of its high-field chemical shift. The observation of this interaction that integrates to one methyl group indicates that one of the phosphines must undergo hindered rotation around the Rh–P bond. The remaining *i*Bu signals in the ^{1}H NMR spectrum are in full accord with this. Notably, six signals in the ratio 3:3:3:3:12:9 (the 12H signal being a 9+3 coincidence) are observed for the remaining isobutyl Me groups. Signals due to the isobutyl phosphine not involved in the agostic interaction become sharper at a lower temperature (253 K). At 200 K the SMe group resolves into a doublet (J(P,H) = 6 Hz), consistent with its orientation *trans* to P1 in the solid-state structure. Selective decoupling of the $\delta = 36.6$ ppm signal in the ^{31}P NMR spectrum makes this signal collapse to a singlet, confirming this assignment (Figure 5). Decoupling the signal at $\delta = 77.4$ ppm does not affect the SMe signal (consistent with a *cis* orientation), but it does simplify the agostic CH_3 resonance to a doublet (J(Rh,P) = 6 Hz). This provides additional confirmation for the agostic Rh···H_3C interaction and its relative orientation on the metal centre, and also assigns the $\delta = 77.4$ ppm resonance to P2, that is, opposite to the agostic interaction, Figure 4. Similar strong correlations between agostic CH_3 groups and *trans*-orientated groups have recently been reported.[40] The signal due to P2 also shows a larger J(Rh,P) coupling constant in the ^{31}P NMR spectrum at low temperature, consistent with it sitting *trans* to a vacant, or at least weakly occupied, site. Warming a solution of **9** in 1,2-$F_2C_6H_4$ resulted in decomposition, although not decomposition to **7**. ESIMS of **8b** and **9** show the expected isotope pattern and masses.

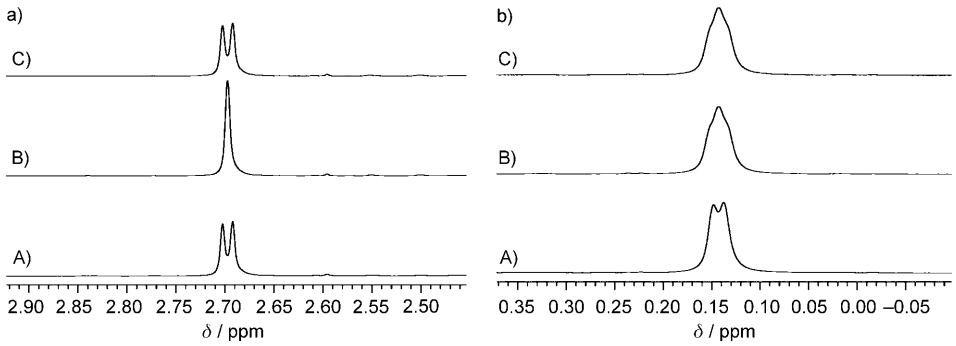

Figure 5. Selected ^{1}H{^{31}P} NMR spectra of **9** showing a) the SMe and b) the agostic Rh···H_3C groups at 200 K (CD_2Cl_2). A) Selectively decoupling the $\delta = 77.4$ ppm (^{31}P) resonance; B) selectively decoupling the $\delta = 36.6$ ppm (^{31}P) resonance; C) the control (off-resonance decoupling), which demonstrates no change.

We have also probed the different fluxional behaviour of **8** and **9** by using DFT calculations on the model complexes **8'** and **9'**. For **8'**, the computed activation barrier for phosphine exchange is only 4.2 kcal mol^{-1}, whereas for **9'** this increases to 10.8 kcal mol^{-1}, a result that is consistent with much lower rate of exchange in the Rh–S system. The transition states for these processes resemble that shown in Scheme 7, and in particular exhibit a lengthening of the Rh–O bond length (from 2.30 Å in **8'** to 2.68 Å) and the Rh–S bond length (from 2.48 Å in **9'** to 2.57 Å).[50] The fact that the Rh–O interaction appears to be intrinsically weaker may, therefore, facilitate the exchange process in **8'** and by extension in **8b**.

The differing behaviour of **8a/b** and **9** in solution can, therefore, be traced back to the stronger Rh–S bond in **9** over the Rh–O bond in **8b** (and presumably also **8a**). This may also be reflected in onward reactivity because **8** goes on to form **7**, whereas **9** is relatively stable. Isolated sigma or agostic C–H interactions such as that observed in **8b** (and further confirmed in **9**), which then undergo C–H activation are relatively rare, especially for late transition metals.[22,27b,29,39,40,51] This coupled with the Rh^{III} oxidation state in the starting material that would disfavour an oxidative addition route prompted us to investigate the mechanism of this C–H activation process by using computational methods.

Computational study of C–H activation in 8b and 9: Calculations on these C–H activation processes were performed for both the model systems **8'** and **9'** and the full experimental complexes **8b** and **9**. In general, results with the full models proved to be more satisfactory and will be discussed in detail here.[52] Calculations on **8b** and **9** were based on the crystallographically determined structures of these species and considered two alternative pathways: 1) σ-bond metathesis (or σ-CAM) and 2) a phosphine-assisted proton transfer in which C–H activation occurs through deprotonation of one of the alkyl C–H bonds geminal to the agostic interaction followed by protonation of the aryl group.[40] The possibility of this second pathway was suggested by the observation of phosphine decomposition products in solution, indicating that phosphine dissociation could be accessible. In the calculations this free phosphine was modelled with PMe_3. A range of alternative mechanisms, including oxidative addition to a Rh^V alkyl hydride, were also assessed, but proved to be much higher in energy.[53]

Computed solvent-corrected reaction profiles for both of the C–H activation pathways of **8b** are shown schematically in Figure 6, with details of the key transition states given in Figure 7. To assess both mechanisms against a common starting geometry an external PMe_3 molecule was included in both pathways (although it was subsequently shown that PMe_3 plays no direct role in the σ-bond metathesis). The σ-bond metathesis mechanism proceeds via **TS(8b-10)** in

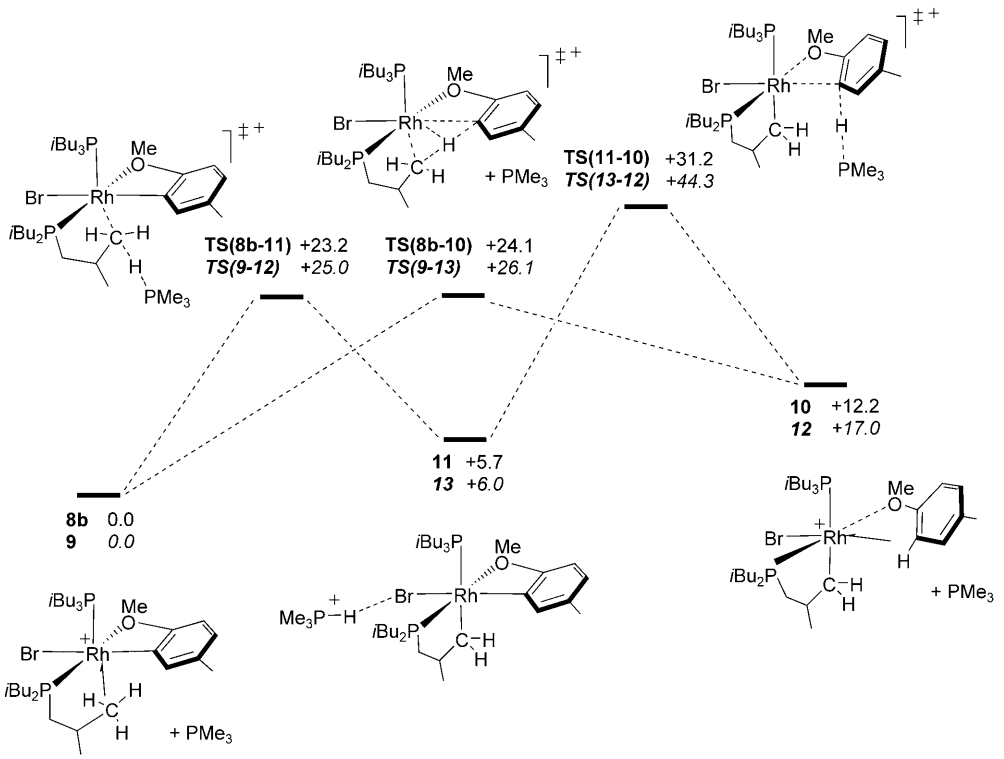

Figure 6. Calculated pathways for C–H activation in **8b** to form **10** in the presence of external PMe_3, corrected for solvation effects in chlorobenzene. The figures in italics refer to the equivalent data for the transformation of thioanisole species **9** to **12**.

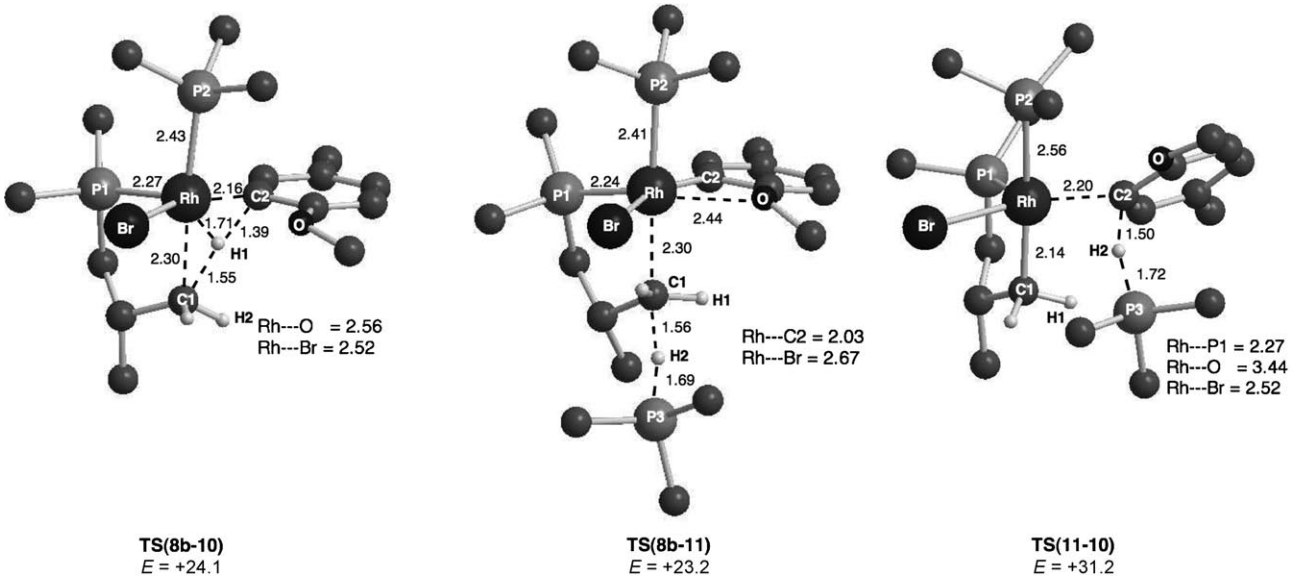

Figure 7. Computed transition states for C–H activation in **8b** highlighting the reacting isobutyl group. Other isobutyl groups are truncated at the α carbon and non-reacting hydrogen atoms are omitted for clarity. Selected bond lengths are reported in Å and the relative energies are reported in kcal mol^{-1}. The external PMe_3 molecule included in the calculation of **TS(8b-10)** is also omitted because it plays no direct role in the σ-bond metathesis transition state.

which the transferring agostic hydrogen, H1, is between the alkyl and aryl carbons (C1···H1 = 1.55 and C2···H1 = 1.39 Å, see Figure 7). In addition, a short Rh···H1 contact of 1.71 Å was computed, typical of σ-bond metathesis processes at late-transition-metal centres.[54,55] Significant elongation of the Rh···O bond length from 2.37 in **8b** to 2.56 Å was also seen. **TS(8b-10)** leads to direct transfer of the agostic hydrogen to the aryl group to form **10** ($E = +12.2$ kcal mol^{-1}),

which features an anisole ligand bound to the metal through both the oxygen (Rh···O = 2.44 Å) and an agostic interaction with the C2–H1 bond (Rh···H1 = 1.95, C2–H1 = 1.13 Å). In **TS(8b-10)** the external PMe_3 is far removed from the reacting centres and is, therefore, omitted from Figure 7.[56] Once formed, **10** could readily lose anisole to access the final cyclometallated dimer **7**. These final products were very stable ($E = -19.5$ kcal mol^{-1}, compare with **8b**), although solvation effects were found to be important in this case with the relative energies of the products being $+10.7$ kcal mol^{-1} in the gas phase. This is presumably due to the 2+ charge of the dimer and for this reason the solvent-corrected energies are presented throughout, although the effect on the values in Figures 6 and 7 was minor (less than 1 kcal mol^{-1}). The fact that both **8b** and **10** are sigma complexes formally identifies this transformation as a σ-CAM mechanism and so the isolation of **8b** is particularly significant. The facile loss of anisole from **10** to form dimeric **7**, however, precludes its isolation.[36]

The alternative phosphine-assisted mechanism involves initial deprotonation of the alkyl C1–H2 bond geminal to the agostic interaction. This proceeds via **TS(8b-11)** (see Figure 7) and exhibits an elongation of the C1···H2 distance to 1.56 Å as it transfers onto PMe_3 (P3···H2 = 1.69 Å). At the same time, the Rh centre approaches C1 (Rh···C1 = 2.30 Å) and an elongation of the Rh···O distance to 2.44 Å is seen. This results in the cyclometallated intermediate **11** ($E = +5.7$ kcal mol^{-1}) in which the phosphonium cation is closely associated with the Br ligand (H2···Br = 2.15 Å). Protonation of the aryl ligand to form **10** then occurs via **TS(11–10)** ($E = +31.2$ kcal mol^{-1}) in which the key distances are similar to those seen for **TS(8b-10)** (C2···H2 = 1.50 and P3···H2 = 1.72 Å). **TS(11–10)** does, however, exhibit the complete disruption of the Rh···O interaction (Rh···O = 3.44 Å) and this may reflect the sterically less accessible nature of this step in which a proton must be delivered to a site bound to the metal, compared with the initial alkyl deprotonation, which occurs remotely from the metal centre. Viewing this second step in reverse indicates that deprotonation of an aryl agostic C–H bond ($\Delta E^{\ddagger} = 19.0$ kcal mol^{-1}) is easier than deprotonation of the alkyl non-agostic C–H bond ($\Delta E^{\ddagger} = 23.2$ kcal mol^{-1}).

Comparison of the two mechanisms shows that σ-bond metathesis is more accessible ($\Delta E^{\ddagger} = 24.1$ kcal mol^{-1}) than the alkyl deprotonation/aryl protonation pathway ($\Delta E^{\ddagger} = 31.2$ kcal mol^{-1}). The high energy of the latter arises from the more difficult aryl protonation step and in fact the initial alkyl deprotonation ($\Delta E^{\ddagger} = 23.2$ kcal mol^{-1}) is competitive with σ-bond metathesis. Reversible formation of **11** could, therefore, occur in solution. The formation of **10** by σ-bond metathesis is also uphill and so should also be reversible; however, the highly favourable loss of anisole and dimer formation will trap out this species and pull the equilibrium through to these observed products.

The energetics for C–H activation in **9** are shown in italics in Figure 6. In this case the transition states for σ-bond metathesis and alkyl deprotonation are both approximately 2.0 kcal mol^{-1} higher than for **8b**. This is consistent with the lack of C–H activation of **9** at room temperature, but suggests that this process may be accessible at higher temperatures. Unfortunately, warming solutions of **9** to 40 °C for 24 h led only to unidentified decomposition products. In general the transition states derived from **9** have similar geometries to those shown in Figure 7 for **8b** and full details are, therefore, reserved for the Supporting Information. One notable difference, however, is that the Rh–S bond length in **9** lengthens by only 0.02 Å in forming **TS(9–12)** and **TS(9–13)**. This compares with elongations of 0.19 Å and 0.07 Å in the oxygen-containing analogues and it may be that the weaker Rh–O interaction noted previously in **8b** allows for greater flexibility and so favours C–H activation in this system by either the σ-bond metathesis or alkyl deprotonation mechanism. Support for this is seen in the aryl protonation step, in which both for **TS(11–10)** (Rh···O = 3.44 Å) and **TS(13–12)** (Rh···S = 3.61 Å) the Rh···O/S interaction is completely broken. The greater energy required to do this in the thioanisole system may account for the difference of 13.1 kcal mol^{-1} in energy between two transition states that are otherwise structurally very similar.

Conclusion

Oxidative addition of aryl bromides to the formally 12-electron Rh^I complexes $[Rh(P\mathit{i}Bu_3)_2][BAr^F_4]$ forms a variety of products. With *m*- and *p*-substituted tolyl bromides the expected dimeric Rh^{III} aryl halides result. In contrast, with sterically encumbered *o*-BrC_6H_4Me the isolated product is one in which the arene has been lost and one isobutyl phosphine substituent has undergone C–H activation. Trapping experiments with anisole or thioanisole bromides indicate a likely intermediate for this process is a low-coordinate Rh^{III} complex that then undergoes C–H activation. The isolation of the sigma complex $[Rh(P\mathit{i}Bu_3)_2(C_6H_4OMe)Br][BAr^F_4]$ and its onward reactivity to give the products of C–H activation and aryl elimination suggest that it is an isolated intermediate in a σ-bond metathesis reaction (formally a σ-CAM transformation), a hypothesis strengthened by DFT calculations. These calculations also rule out oxidative addition and suggest that phosphine-assisted alkyl deprotonation is a competitive reversible side reaction.

Experimental Section

General methods and materials: All manipulations, unless otherwise stated, were performed under an atmosphere of argon by using standard Schlenk and glove-box techniques. Glassware was oven dried at 130 °C overnight and flamed under vacuum prior to use. CH_2Cl_2, MeCN and pentane were dried by using a Grubbs-type solvent purification system (MBraun SPS-800) and degassed by successive freeze–pump–thaw cycles.[57] CD_2Cl_2, C_6H_5F and 1,2-$C_6H_4F_2$ were distilled under vacuum from CaH_2 and stored over 3 Å molecular sieves. All other liquid substrates were degassed by freeze–pump–thaw cycles and stored under argon over 3 Å molecular sieves. Solid substrates were used as received

from the supplier. $[Rh(PiBu_3)_2][BAr^F_4]$,[8] $[Rh(PiBu_3)_2(C_6H_5F)][BAr^F_4]$[8] and $Na[BAr^F_4]$[58] were prepared by using the literature methods. NMR spectra were recorded on a Bruker AVII 500 MHz or a Varian Unity+ 500 MHz spectrometer at room temperature unless otherwise stated. All samples, deuterated and non-deuterated samples were locked and referenced to CD_2Cl_2 (^1H $\delta = 5.32$ ppm). Chemical shifts are quoted in ppm and coupling constants in Hz (v = virtual). All NMR data were taken at 293 K unless otherwise stated. Mass Spectrometry was carried out on a Bruker micrOTOF-Q interfaced with a glove box or Bruker micrOTOF both interfaced to a glove box.[59]

X-ray crystallography: For all X-ray crystallographic and chemical diagrams, assume the presence of the $[BAr^F_4]^-$ anion when not shown. Data were acquired on a Nonius Kappa CCD diffractometer using graphite monochromated $Mo_{K\alpha}$ radiation ($\lambda = 0.71073$ Å) and a low-temperature device (150 K);[60] data were collected by using COLLECT and reduction and cell refinements were performed by using DENZO/SCALEPACK.[61] The structures were solved by direct methods by using SHELX-97 (**4**)[62] or SIR2004 (**5**, **6**, **8b** and **9**),[63] or Patterson interpretation by using SHELX-86 (**7**).[62] Structures were refined by using full-matrix least-squares on F^2 by using SHELXL-97 in all cases with the exception of **8b**, which was refined with a two-component twin law (0.7781(16) and 0.2219(16) occupancy, see the cif file for full details) by using CRYSTALS.[64] Non-hydrogen atoms were refined anisotropically. The hydrogen atoms H3A and H3B in **7** were located in the difference map and were freely refined; their isotropic displacement parameters were fixed to ride on the parent atom. All other hydrogen atoms were placed in calculated positions by using the riding model. For **8b** the position of hydrogen atoms and the isotropic displacement parameters were refined separately with soft restraints prior to inclusion in the refinement by using a riding model.

Disorder of the phosphine ligands in **5**, **6** and **7** was treated by modelling the appropriate substituents over two or three sites and restraining their geometry. Rigid body restraints were applied to the arene rings of both independent difluorobenzene molecules in **5** and restraints to the C–F bond lengths were also applied. The occupancy of each molecule was modelled at 50% and one of the difluorobenzene molecules lies on a special position. Rotational disorder of the anion CF_3 groups was treated by modelling the fluorine atoms or the entire CF_3 group over two sites and restraining their geometry.

A minor contribution from a conformational isomer of the cation in **7** (less than 6%) can be detected in the difference map during the refinement and gives rise to significant peaks surrounding Rh1 (2.19, 1.09 and 1.07 e Å^{-3}) in a similar manner to the structure of $[Rh(PiBu_3)_2PhBr]_2^{2+}$.[8] Modelling this disorder was unsuccessful and only the major component was subsequently refined. In the absence of the three aforementioned peaks, the highest peak was 0.68 e Å^{-3} giving a max/min ratio of 0.7. Restraints to thermal parameters were applied where necessary to maintain sensible values. Images were generated by using CrystalMaker. A summary of the crystal data for complexes **4**–**9** is given in Table 3. CCDC-768006 (**4**), 768007 (**5**), 768008 (**6**), 768009 (**7**), 768010 (**8b**) and 768011 (**9**) contain the supplementary crystallographic data for this paper. These data can be obtained free of charge from The Cambridge Crystallographic Data Centre via www.ccdc.cam.ac.uk/data_request/cif.

Computational details: All DFT calculations were run with Gaussian 03[65] using the BP86 functional. Rh, P and Br centres were described with the Stuttgart RECPs and associated basis sets,[66] with added d-orbital polarisation on P and Br.[67] 6–31G** basis sets were used for all other atoms.[68] All stationary points were fully characterised through analytical frequency calculations as either minima (all positive eigenvalues) or transition states (one imaginary eigenvalue) and intrinsic reaction coordinate (IRC) calculations and subsequent geometry optimisations were used to confirm the minima linked by each transition state. All reported energies include a correction for zero-point energies and those in the C–H activation study are also corrected for solvation effects through the PCM method. In the absence of parameters for fluorobenzene ($\varepsilon = 5.4$) used experimentally, chlorobenzene ($\varepsilon = 5.7$) was employed.[65]

Synthesis of 4: C_6H_5F (5 mL) was added to a Schlenk flask containing $[Rh(PiBu_3)_2(C_6H_5F)][BAr^F_4]$ (0.088 g, 0.064 mmol) and *p*-C_6H_4ClBr (0.123 g, 0.64 mmol). The orange solution was left for 1.5 h during which time an orange powder precipitated, which was isolated by decantation and washed with pentane (3×5 mL). Yield: 0.048 g (47% based in Rh). Crystals were obtained by layering a 1,2-$C_6H_4F_2$ solution of product and

Table 3. Crystallographic data for **4**–**9**.

	4	**5**	**6**	**7**	**8b**	**9**
formula	$C_{136}H_{148}B_2Br_2Cl_2F_{52}P_4Rh_2$	$C_{132}H_{150}B_2Br_2F_{50}P_4Rh_2$	$C_{138}H_{154}B_2Br_2F_{52}P_4Rh_2$	$C_{112}H_{130}B_2Br_2F_{48}P_4Rh_2$	$C_{64}H_{75}BBrF_{24}OP_2Rh$	$C_{63.50}H_{74}BBrClF_{24}P_2RhS$
M_r	3352.58	3197.66	3311.75	2899.30	1571.82	1616.31
crystal system	triclinic	triclinic	monoclinic	triclinic	monoclinic	monoclinic
space group	$P\bar{1}$	$P\bar{1}$	$C2/c$	$P\bar{1}$	Pn	$P2_1/c$
a [Å]	13.12230(10)	16.9040(2)	31.4243(3)	13.4951(2)	13.0267(2)	27.6187(2)
b [Å]	14.0207(2)	21.7096(3)	13.61470(10)	14.2999(2)	27.3217(5)	12.90720(10)
c [Å]	21.4584(3)	21.8369(2)	36.9083(3)	17.9959(3)	19.7871(3)	40.9486(3)
α [°]	72.0163(6)	77.7399(7)	–	101.3541(5)	–	–
β [°]	83.8320(6)	72.0851(7)	110.6315(4)	108.1093(5)	90.7348(12)	99.1088(3)
γ [°]	84.3323(6)	71.0422(5)	–	97.8670(5)	–	–
V [Å^3]	3724.39(8)	7155.05(14)	14777.8(2)	3162.25(8)	7041.9(2)	14413.28(18)
Z	1	2 ($Z'=2$)	4	1	4 ($Z'=2$)	8 ($Z'=2$)
ρ [g cm^{-3}]	1.495	1.484	1.489	1.522	1.483	1.490
μ [mm^{-1}]	0.948	0.945	0.920	1.059	0.958	1.001
θ range [°]	$5.11 \le \theta \le 26.37$	$5.11 \le \theta \le 26.37$	$5.10 \le \theta \le 26.37$	$5.11 \le \theta \le 26.37$	$5.104 \le \theta \le 26.052$	$5.08 \le \theta \le 26.37$
reflns collected (R_{int})	26324 (0.0310)	46782 (0.0324)	22164 (0.0256)	21758 (0.0244)	55067 (0.082)	40752 (0.0299)
no. of data/restraints/parameters	15116/60/954	28594/906/2194	14418/424/1092	12808/687/919	21094/230/1802	27215/918/1899
R_1 [$I > 2\sigma(I)$]	0.0435	0.0991	0.0550	0.0437	0.0777	0.0498
wR_2 (all data)	0.1175	0.2382	0.1442	0.1112	0.1998	0.1161
GoF	1.038	1.149	1.016	1.023	0.9613	1.017
largest difference peak and hole [e Å^{-3}]	0.823, −0.707	1.868, −1.671	1.058, −0.560	2.192, −0.981	2.52, −2.03	0.777, −0.834

pentane at room temperature. The dication salt is only sparingly soluble in CD_2Cl_2 and thus NMR spectra were recorded in 1,2-$C_6H_4F_2$, a solvent in which it has moderate solubility. ^{1}H NMR (1,2-$C_6H_4F_2$, 500 MHz): $\delta =$ 8.26 (s, 16H; B*Ar*$^F_4$), 7.61 (s, 8H; B*Ar*$^F_4$), other aromatic resonances were obscured owing to the protio solvent, 2.23 (brs, 24H; PC*H*$_2$CHMe$_2$), 2.16 (brs, 12H; PCH$_2$C*H*Me$_2$), 1.25 (brs, 36H; PCH$_2$CH*Me*$_2$), 1.05 ppm (brs, 36H; PCH$_2$CH*Me*$_2$); ^{31}P{^{1}H} NMR (1,2-$C_6H_4F_2$, 202 MHz): $\delta = 44.4$ ppm (d, J(Rh,P) = 139 Hz); ESIMS (1,2-$C_6H_4F_2$, 60 °C, 4.5 kV): m/z: calcd for $[Rh(C_6H_4Cl)Br(P\textit{i}Bu_3)_2]^+$: 699.1915; found: 699.1918; elemental analysis calcd (%) for $C_{124}H_{140}B_2Br_2Cl_2F_{48}P_4Rh_2$: H 4.52, C 47.7; found: H 4.37, C 48.1

Synthesis of 5: C_6H_5F (2 mL) was added to a Schlenk flask containing $[Rh(P\textit{i}Bu_3)_2(C_6H_5F)][BAr^F_4]$ (0.078 g, 0.053 mmol) and *p*-$C_6H_4Br(CH_3)$ (0.090 g, 0.53 mmol). The resulting solution was left to stand at room temperature for 2 h during which time an orange precipitate formed. The orange powder was isolated by decantation and washed with pentane (3 × 5 mL). Yield: 0.057 g (70%). Crystals were obtained from a 1,2-$C_6H_4F_2$/pentane layer. ^{1}H NMR (CD_2Cl_2, 500 MHz): $\delta = 7.72$ (s, 16H; B*Ar*$^F_4$), 7.56 (s, 8H; B*Ar*$^F_4$), 7.03 (d, 4H, J(H,H) = 8 Hz; H^2), 6.89 (d, 4H, J(H,H) = 8 Hz; H^3), 2.34 (s, 6H; Ar*Me*), 2.08 (s, 24H; PC*H*$_2$CHMe$_2$), 2.05–1.95 (brm, 12H; PCH$_2$C*H*Me$_2$), 1.12 (d, 36H, J(H,H) = 6 Hz; PCH$_2$CH*Me*$_2$), 1.02 ppm (d, 36H, J(H,H) = 6 Hz; PCH$_2$CH*Me*$_2$); ^{13}C{^{1}H} NMR (CD_2Cl_2, 126 MHz): $\delta = 162.3$ (q, J(B,C) = 50 Hz; B*Ar*$^F_4$), 138.9 (s; C^4), 137.8 (s; C^3 or C^2), 135.4 (s; B*Ar*$^F_4$), 130.8 (s; C^3 or C^2), 129.4 (q, J(F,C) = 32 Hz; B*Ar*$^F_4$), 125.3 (d, J(Rh,C) = 5 Hz; C^1), 125.2 (q, J(F,C) = 272 Hz; B*Ar*$^F_4$), 118.2–117.8 (m; B*Ar*$^F_4$), 36.6–36.4 (m; PC*H*$_2$CHMe$_2$), 26.6 (s; PCH$_2$C*H*Me$_2$), 26.1 (s; PCH$_2$CH*Me*$_2$), 25.9 (s; PCH$_2$CH*Me*$_2$), 20.6 ppm (s; Ar*CH*$_3$); ^{31}P{^{1}H} NMR (CD_2Cl_2, 122 MHz): $\delta = 40.2$ ppm (d, J(Rh,P) = 138 Hz); ESIMS (CH_2Cl_2, 60 °C, 4.5 kV): m/z: calcd for $[Rh(P\textit{i}Bu_3)_2\{C_6H_4(CH_3)Br\}]^+$: 679.2463; found: 679.2496; elemental analysis calcd (%) for $C_{126}H_{146}B_2Br_2F_{48}P_4Rh_2$: H 4.02, C 49.08; found: H 4.48, C 49.65.

Synthesis of 6: C_6H_5F (2 mL) and *m*-C_6H_4MeBr (85 μL) were added to a Schlenk flask containing $[Rh(P\textit{i}Bu_3)_2(C_6H_5F)][BAr^F_4]$ (0.101 g, 0.069 mmol) and were left for 2 h during which time an orange powder precipitated. This was isolated by decantation and washed with pentane (3 × 5 mL). Yield: 0.064 g (60% based on Rh). Crystals were obtained from a C_6H_5F/pentane layer. ^{1}H NMR (CD_2Cl_2, 500 MHz): $\delta = 7.72$ (brs, 16H; B*Ar*$^F_4$), 7.56 (s, 8H; B*Ar*$^F_4$), 7.07–6.89 (4 × m, 8H; *Ar*), 2.31 (s, 6H; Ar*Me*), 2.15–2.05 (brm, 24H; PC*H*$_2$CHMe$_2$), 2.05–1.95 (m, 12H; PCH$_2$C*H*Me$_2$), 1.12 (d, J(H,H) = 7 Hz, 36H; PCH$_2$CH*Me*$_2$), 1.02 ppm (d, J(H,H) = 7 Hz, 36H; PCH$_2$CH*Me*$_2$); ^{13}C{^{1}H} NMR (CD_2Cl_2, 126 MHz): $\delta = 162.3$ (q, J(B,C) = 50 Hz; B*Ar*$^F_4$), 152.0 (s; C^{Ar}), 150.1 (s; C^{Ar}), 140.4 (s; C^{Ar}), 138.2 (s; C^{Ar}), 135.3 (s; B*Ar*$^F_4$), 129.52 (s; C^{Ar}), 129.42 (q, J-(F,C) = 32 Hz; B*Ar*$^F_4$), 125.14 (q, J(F,C) = 272 Hz, CF$_3$; B*Ar*$^F_4$), 125.27 (s; C^{Ar}), 118.2–117.8 (m; B*Ar*$^F_4$), 36.53 (brs; PC*H*$_2$CHMe$_2$), 26.59 (s; PCH$_2$C*H*Me$_2$), 26.11 (s; PCH$_2$CH*Me*$_2$), 25.84 (s; PCH$_2$CH*Me*$_2$), 22.06 ppm (s; Ar*CH*$_3$); ^{31}P{^{1}H} NMR (CD_2Cl_2, 122 MHz): $\delta = 40.8$ ppm (d, J(Rh,P) = 139 Hz); ESIMS (CH_2Cl_2, 60 °C, 4.5 kV): m/z: calcd for $[Rh(P\textit{i}Bu_3)_2(C_6H_4(CH_3)Br]^+$: 677.2481; found: 677.2594; elemental analysis calcd (%) for $C_{126}H_{146}B_2Br_2P_4Rh_2F_{48}$: H 4.02, C 49.08; found: H 4.61, C 49.1.

Synthesis of 7: 2-Bromotoluene (10 μL) was added to an NMR tube containing $[Rh(P\textit{i}Bu_3)_2][BAr^F_4]$ (0.010 g, 0.0073 mmol) and C_6H_5F (550 μL). The sample turned from orange to orange/brown when left for 16 h at room temperature. Crystalline material was obtained by crystallisation from C_6H_5F/pentane. Complex **7** is sparingly soluble in CD_2Cl_2 and NMR analysis was performed in C_6H_5F. Toluene was identified as a product of the reaction by GC–MS. Complex **7** could not be prepared in an analytically pure form, despite repeated attempts. Yield (95% pure material as determined by ^{1}H NMR spectroscopy) = 0.005 g (47%); ^{1}H NMR (C_6H_5F, 500 MHz): $\delta = 8.51$ (s, 16H; BAr$^F_4$), 7.84 (s, 8H; BAr$^F_4$), 4.45 and 4.30 (2 × s, 2H; ratio major/minor ≈ 1:2), 3.25 and 3.15 (2 × s, 2H; major/minor ≈ 1:2), 2.70–1.70 (m, ≈ 34H), 1.37 (brs, ≈ 12H), 1.20–1.00 ppm (brm, ≈ 56H); ^{31}P{^{1}H} NMR (C_6H_5F, 202 MHz): $\delta = 58.0$ (dd, J(Rh,P) = 140 Hz, J(P,P) = 28 Hz; minor isomer, ratio major/minor 1:2), 55.4 (dd, J(Rh,P) = 142 Hz, J(P,P) = 28 Hz), 37.8 (dd, J(Rh,P) = 143 Hz, J(P,P) = 28 Hz; minor isomer, ratio major/minor 1:2), 37.0 ppm (dd, J(Rh,P) = 142 Hz, J(P,P) = 28 Hz); ESIMS (C_6H_5F, 60 °C, 4.5 kV): m/z: calcd for $[Rh(P\textit{i}Bu_3)_2(P\textit{i}Bu_2C_4H_8)_2Br_2]^{2+}$: 586.1848; found: 586.1851.

Synthesis of 8b: 2-Bromo-4-methylanisole (58 μL) was added to a Schlenk flask containing $[Rh(P\textit{i}Bu_3)_2][BAr^F_4]$ (0.0550 g, 0.040 mmol) and C_6H_5F (4 mL), and the solution left for 3 h at room temperature during which time a colour change from orange to dark-red was observed. A solid was isolated by removal of the solvent in vacuo and washing with pentane (3 × 5 mL). Yield: 0.0387 g (62%). Crystals were obtained from a C_6H_5F/pentane layer. Complex **8b** is unstable with respect to the formation of **7** as the major organometallic product over the course of 1 week in solution at room temperature. We were thus unable to obtain good microanalytical data. Use of 2-bromoanisole resulted in a similar product, **8a**, although crystalline material could not be obtained. Anisole was identified as a product by GC–MS in this case. ^{1}H NMR (CD_2Cl_2, 500 MHz): $\delta = 7.72$ (s, 8H; B*Ar*$^F_4$), 7.56 (s, 4H; B*Ar*$^F_4$), 7.06 (d, 1H, J-(H,H) = 8 Hz; *H*^{3}), 6.81 (s, 1H; *H*^{4}), 6.61 (d, 1H, J(H,H) = 8 Hz; *H*^{4}), 3.99 (s, 3H; O*Me*), 2.33 (s, 3H; Ar*Me*), 2.22–2.07 (m, 6H; PCH$_2$C*H*Me$_2$), 2.07–2.00 (m, 12H; PC*H*$_2$CHMe$_2$), 1.14 (d, 18H, J(H,H) = 6 Hz; CH$_2$CH*Me*$_2$), 1.02 ppm (d, 18H, J(H,H) = 6 Hz; CH$_2$CH*Me*$_2$), the signal at 2.07–2.00 resolves into 2 × 6H multiplets at 200 K at $\delta = 1.95$ and 2.05 ppm; ^{13}C{^{1}H} NMR (CD_2Cl_2, 126 MHz): $\delta = 166.5$ (s; C^2), 162.3 (q, J-(B,C) = 50 Hz; B*Ar*$^F_4$), 136.2 (s; C^5), 135.4 (s; B*Ar*$^F_4$), 133.2 (s; C^6), 130.6 (d, J(Rh,C) = 8 Hz; C^1), 129.5 (s; C^4), 129.4 (q, J(F,C) = 32 Hz; B*Ar*$^F_4$), 125.2 (q, J(F,C) = 272 Hz; B*Ar*$^F_4$), 118.0 (s; B*Ar*$^F_4$), 112.8 (s; C^3), 60.26 (s; ArO*Me*), 39.2–38.0 (m; PC*H*$_2$CHMe$_2$), 26.4 (s; PCH$_2$CH*Me*$_2$), 26.1 (brs; PCH$_2$C*H*Me$_2$), 25.5 (s; PCH$_2$CH*Me*$_2$), 21.8 ppm (s; Ar*CH*$_3$); ^{31}P{^{1}H} NMR (CD_2Cl_2, 202 MHz): $\delta = 65.7$ ppm (d, J(Rh,P) = 156 Hz), there was no appreciable change in the spectra apart from a slight broadening on cooling to 200 K; ESIMS (CH_2Cl_2, 60 °C, 4.5 kV): m/z: calcd for $[Rh(P\textit{i}Bu_3)_2C_6H_4(CH_3)(OCH_3)Br]^+$: 709.2569; found: 709.2606.

Synthesis of 9: 2-bromothioanisole (7 μL) was added to a Schlenk flask containing $[Rh(P\textit{i}Bu_3)_2][BAr^F_4]$ (0.0333 g, 0.024 mmol) and C_6H_5F (4 mL) and the solution was left to stand for 1.5 h during which time a colour change from orange to dark red was observed. Removal of the solvent in vacuo and washing with pentane (3 × 5 mL, ultrasound bath) afforded red crystals of **9**. Yield: 0.0216 g (56%). Recrystallisation from CH_2Cl_2/pentane afford X-ray quality crystals. Complex **9** is considerably more stable than **8** at room temperature, but decomposes on warming to above 40 °C. ^{1}H NMR (CD_2Cl_2, 500 MHz, 293 K): $\delta = 7.72$ (s, 8H; B*Ar*$^F_4$), 7.56 (s, 4H; B*Ar*$^F_4$), 7.40 (vtd, 1H, J(H,H) = 7.7 or 1.5 Hz; H^4 or H^5), 7.34 (vtd, 1H, J-(H,H) = 7.7 or 1.5 Hz; H^4 or H^5), 7.28 (d, 1H, J(H,H) = 7.7 Hz; H^3 or H^6), 7.09 (dd, 1H, J(H,H) = 7 or 1.5; H^3 or H^6), 2.78 (vt, 3H, J(P,H) = 2 Hz; ArS*Me*), 2.5–1.70 (brm, 18H; PC*H*$_2$C*H*Me$_2$), 1.05 (brs, 18H; PCH$_2$CH*Me*$_2$), 0.93 ppm (brs, 18H; PCH$_2$CH*Me*$_2$); ^{13}C{^{1}H} NMR (CD_2Cl_2, 126 MHz, 293 K): $\delta = 162.30$ (q, J(B,C) = 50 Hz; B*Ar*$^F_4$), 141.9 (brs; C^1), 141.9 (s; C^2), 135.5 (s; B*Ar*$^F_4$), 133.3 (s; C^3), 133.0 (s; C^5), 130.8 (s; C^6), 129.6 (s; C^4), 129.4 (q, J(F,C) = 32 Hz; B*Ar*$^F_4$), 125.2 (q, J(F,C) = 272 Hz; B*Ar*$^F_4$), 118.0 (brs; B*Ar*$^F_4$), 26.5–25.24 (m; P*iBu*$_3$), 25.07 ppm (s; S*CH*$_3$); ^{31}P{^{1}H} NMR (C_6H_5F, 202 MHz, 293 K): $\delta = 77.1$ (d, J(Rh,P) = 150 Hz), 34.6 ppm (d, J(Rh,P) = 145 Hz); ESIMS (CH_2Cl_2, 60 °C, 4.5 kV): m/z: calcd for $[Rh(P\textit{i}Bu_3)_2\{C_6H_4SCH_3Br\}]^+$: 711.2183; found: 711.2090; elemental analysis calcd (%) for $C_{63}H_{73}BBrF_{24}SP_2Rh{\cdot}CH_2Cl_2$: H 4.56, C 46.3; found: H 4.44, C 47.2; ^{1}H NMR (CD_2Cl_2, 500 MHz, 200 K): $\delta = 7.71$ (s, 8H; B*Ar*$^F_4$), 7.53 (s, 4H; B*Ar*$^F_4$), 7.34 (t, 1H, J(H,H) = 7.7 Hz; H^4 or H^5), 7.24 (t, 1H, J(H,H) = 7.7 Hz; H^4 or H^5), 7.18 (t, 1H, J(H,H) = 7.7 Hz; H^3 or H^6), 7.03 (t, 1H, J(H,H) = 7.7 Hz; H^3 or H^6), 2.71 (d, 2H, J-(Rh,H) or J(P,H) = 6 Hz; ArS*Me*), 2.42–2.34 (brm, 2H; CH), 2.24–2.18 (brm, 3H), 2.05–1.80 (brm, 13H), 1.24 (d, 3H, J(H,H) = 6 Hz; PCH$_2$CH*Me*$_2$), 1.13 (d, 3H, J(H,H) = 6 Hz; PCH$_2$CH*Me*$_2$), 1.06 (d, 3H, J-(H,H) = 6 Hz; PCH$_2$CH*Me*$_2$), 1.04 (d, 3H, J(H,H) = 6 Hz; PCH$_2$CH*Me*$_2$), 0.92 (brd, 12H, J(H,H) = 6 Hz; PCH$_2$CH*Me*$_2$), 0.78 (brs, 9H; PCH$_2$CH*Me*$_2$), 0.145 ppm (brdd, 3H; Rh···H$_3$C); ^{31}P{^{1}H} NMR (CD_2Cl_2, 202 MHz, 200 K): $\delta = 77.4$ (dd, J(Rh,P) = 151.9 Hz, J(P,P) = 20.4 Hz), 36.6 (dd, J(Rh,P) = 131.5 ppm, J(P,P) = 20.3 Hz).

[1] M. Portnoy, D. Milstein, *Organometallics* **1993**, *12*, 1665–1673; J. P. Stambuli, C. D. Incarvito, M. Bühl, J. F. Hartwig, *J. Am. Chem. Soc.*

2004, *126*, 1184–1194; F. Barrios-Landeros, J. F. Hartwig, *J. Am. Chem. Soc.* **2005**, *127*, 6944–6945; J. P. Corbet, G. Mignani, *Chem. Rev.* **2006**, *106*, 2651–2710; O. Esposito, P. M. P. Gois, A. Lewis, S. Caddick, F. G. N. Cloke, P. B. Hitchcock, *Organometallics* **2008**, *27*, 6411–6418; N. Marion, S. P. Nolan, *Acc. Chem. Res.* **2008**, *41*, 1440–1449; R. Martin, S. L. Buchwald, *Acc. Chem. Res.* **2008**, *41*, 1461–1473; B. P. Fors, N. R. Davis, S. L. Buchwald, *J. Am. Chem. Soc.* **2009**, *131*, 5766–5768.

[2] F. Barrios-Landeros, B. P. Carrow, J. F. Hartwig, *J. Am. Chem. Soc.* **2009**, *131*, 8141–8154; T. E. Barder, S. D. Walker, J. R. Martinelli, S. L. Buchwald, *J. Am. Chem. Soc.* **2005**, *127*, 4685–4696; U. Christmann, R. Vilar, *Angew. Chem.* **2005**, *117*, 370–378; *Angew. Chem. Int. Ed.* **2005**, *44*, 366–374; A. K. de K. Lewis, S. Caddick, F. G. N. Cloke, N. C. Billingham, P. B. Hitchcock, J. Leonard, *J. Am. Chem. Soc.* **2003**, *125*, 10066–10073.

[3] J. C. Green, B. J. Herbert, R. Lonsdale, *J. Organomet. Chem.* **2005**, *690*, 6054–6067; M. Ahlquist, P.-O. Norrby, *Organometallics* **2007**, *26*, 550–553.

[4] V. V. Grushin, H. Alper, *Chem. Rev.* **2002**, *102*, 1047–1062; V. V. Grushin, W. J. Marshall, *J. Am. Chem. Soc.* **2004**, *126*, 3068–3069; L. Fan, S. Parkin, O. V. Ozerov, *J. Am. Chem. Soc.* **2005**, *127*, 16772–16773; S. Gatard, R. Celenligil-Cetin, C. Y. Guo, B. M. Foxman, O. V. Ozerov, *J. Am. Chem. Soc.* **2006**, *128*, 2808–2809; J.-i. Ito, T. Miyakawa, H. Nishiyama, *Organometallics* **2008**, *27*, 3312–3315; C. Douvris, C. A. Reed, *Organometallics* **2008**, *27*, 807–810.

[5] S. T. H. Willems, P. H. M. Budzelaar, N. N. P. Moonen, R. de Gelder, J. M. M. Smits, A. W. Gal, *Chem. Eur. J.* **2002**, *8*, 1310–1320.

[6] K. Ueura, T. Satoh, M. Miura, *Org. Lett.* **2005**, *7*, 2229–2231; Z. Liang, W. Jie, *Adv. Synth. Catal.* **2008**, *350*, 2409–2413; T. Ishiyama, J. Hartwig, *J. Am. Chem. Soc.* **2000**, *122*, 12043–12044; J. C. Lewis, A. M. Berman, R. G. Bergman, J. A. Ellman, *J. Am. Chem. Soc.* **2008**, *130*, 2493–2500; X. Wang, B. S. Lane, D. Sames, *J. Am. Chem. Soc.* **2005**, *127*, 4996–4997; J. C. Lewis, R. G. Bergman, J. A. Ellman, *Acc. Chem. Res.* **2008**, *41*, 1013–1025.

[7] V. V. Grushin, H. Alper, *Organometallics* **2002**, *21*, 1620–1622; M. A. Esteruelas, J. Herrero, M. Olivan, *Organometallics* **2004**, *23*, 3891–3897.

[8] T. M. Douglas, A. B. Chaplin, A. S. Weller, *Organometallics* **2008**, *27*, 2918–2921.

[9] M. J. Ingleson, S. K. Brayshaw, M. F. Mahon, G. D. Ruggiero, A. S. Weller, *Inorg. Chem.* **2005**, *44*, 3162–3171.

[10] N. M. Scott, V. Pons, E. D. Stevens, D. M. Heinekey, S. P. Nolan, *Angew. Chem.* **2005**, *117*, 2568–2571; *Angew. Chem. Int. Ed.* **2005**, *44*, 2512–2515.

[11] A. C. Cooper, E. Clot, J. C. Huffman, W. E. Streib, F. Maseras, O. Eisenstein, K. G. Caulton, *J. Am. Chem. Soc.* **1998**, *120*, 97–106.

[12] H_2 loss from related neutral [$Ir(PR_3)_2H_2(CCR')$] systems has also been reported, see ref. [19].

[13] T. M. Douglas, A. B. Chaplin, A. S. Weller, X. Yang, M. B. Hall, *J. Am. Chem. Soc.* **2009**, *131*, 15440–15456.

[14] T. M. Douglas, A. B. Chaplin, A. S. Weller, *J. Am. Chem. Soc.* **2008**, *130*, 14432–14433.

[15] A. B. Chaplin, A. S. Weller, *Angew. Chem.* **2010**, *122*, 591–594; *Angew. Chem. Int. Ed.* **2010**, *49*, 581–584.

[16] T. M. Douglas, **2009**, PhD Thesis, University of Oxford (UK).

[17] H. Wu, M. B. Hall, *Dalton Trans.* **2009**, 5933–5942.

[18] F. Paul, J. Patt, J. F. Hartwig, *Organometallics* **2002**, *21*, 3030–3039; R. B. Biscoe, T. E. Barder, S. L. Buchwald, *Angew. Chem.* **2007**, *119*, 7370–7373; *Angew. Chem. Int. Ed.* **2007**, *46*, 7232–7235; A. G. Sergeev, A. Zapf, A. Spannenberg, M. Beller, *Organometallics* **2008**, *27*, 297–300.

[19] A. C. Cooper, J. C. Huffman, K. G. Caulton, *Organometallics* **1997**, *16*, 1974–1978.

[20] M. Brookhart, M. L. H. Green, G. Parkin, *Proc. Natl. Acad. Sci. USA* **2007**, *104*, 6908–6914.

[21] W. Baratta, C. Mealli, E. Herdtweck, A. Ienco, S. A. Mason, P. Rigo, *J. Am. Chem. Soc.* **2004**, *126*, 5549–5562.

[22] N. M. Scott, R. Dorta, E. D. Stevens, A. Correa, L. Cavallo, S. P. Nolan, *J. Am. Chem. Soc.* **2005**, *127*, 3516–3526.

[23] J. N. Coalter, J. C. Huffman, W. E. Streib, K. G. Caulton, *Inorg. Chem.* **2000**, *39*, 3757–3764.

[24] E. Clot, O. Eisenstein, T. Dube, J. W. Faller, R. H. Crabtree, *Organometallics* **2002**, *21*, 575–580.

[25] B. Holger, R. Krzysztof, U. Katharina, *Chem. Eur. J.* **2008**, *14*, 7858–7866, and references therein.

[26] X.-L. Luo, G. J. Kubas, C. J. Burns, R. J. Butcher, J. C. Bryan, *Inorg. Chem.* **2002**, *41*, 6538–6545.

[27] D. L. Thorn, *Organometallics* **1998**, *17*, 348–352; M. J. Ingleson, M. F. Mahon, A. S. Weller, *Chem. Commun.* **2004**, 2398–2399.

[28] L. A. Labios, M. D. Millard, A. L. Rheingold, J. S. Figueroa, *J. Am. Chem. Soc.* **2009**, *131*, 11318–11319.

[29] B. Rybtchinski, L. Konstantinovsky, L. J. W. Shimon, A. Vigalok, D. Milstein, *Chem. Eur. J.* **2000**, *6*, 3287–3292.

[30] H. A. Y. Mohammad, J. C. Grimm, K. Eichele, H.-G. Mack, B. Speiser, F. Novak, M. G. Quintanilla, W. C. Kaska, H. A. Mayer, *Organometallics* **2002**, *21*, 5775–5784; R. Dorta, R. Goikhman, D. Milstein, *Organometallics* **2003**, *22*, 2806–2809; D. Conner, K. N. Jayaprakash, T. R. Cundari, T. B. Gunnoe, *Organometallics* **2004**, *23*, 2724–2733; A. Y. Verat, M. Pink, H. Fan, J. Tomaszewski, K. G. Caulton, *Organometallics* **2007**, *26*, 166–168.

[31] R. F. R. Jazzar, S. A. Macgregor, M. F. Mahon, S. P. Richards, M. K. Whittlesey, *J. Am. Chem. Soc.* **2002**, *124*, 4944–4945; S. Burling, B. M. Paine, D. Nama, V. S. Brown, M. F. Mahon, T. J. Prior, P. S. Pregosin, M. K. Whittlesey, J. M. J. Williams, *J. Am. Chem. Soc.* **2007**, *129*, 1987–1995; C. Y. Tang, W. Smith, D. Vidovic, A. L. Thompson, A. B. Chaplin, S. Aldridge, *Organometallics* **2009**, *28*, 3059–3066; S. Burling, E. Mas-Marzá, J. E. V. Valpuesta, M. F. Mahon, M. K. Whittlesey, *Organometallics* **2009**, *28*, 6676–6686.

[32] L. Dahlenburg, N. Hock, *Inorg. Chim. Acta* **1985**, *104*, L29–L30.

[33] R. H. Crabtree, *J. Chem. Soc. Dalton Trans.* **2001**, 2437–2450; G. J. Kubas, *Metal Dihydrogen and σ-Bond Complexes*, Kluwer, New York, **2001**.

[34] D. Balcells, E. Clot, O. Eisenstein, *Chem. Rev.* **2010**, *110*, 749–823.

[35] B. A. Vastine, M. B. Hall, *Coord. Chem. Rev.* **2009**, *253*, 1202–1218.

[36] R. N. Perutz, S. Sabo-Etienne, *Angew. Chem.* **2007**, *119*, 2630–2645; *Angew. Chem. Int. Ed.* **2007**, *46*, 2578–2592.

[37] Y. Boutadla, D. L. Davies, S. A. Macgregor, A. I. Poblador-Bahamonde, *Dalton Trans.* **2009**, 5820–5831.

[38] D. L. Davies, S. M. A. Donald, S. A. Macgregor, *J. Am. Chem. Soc.* **2005**, *127*, 13754–13755.

[39] A. Vigalok, O. Uzan, L. J. W. Shimon, Y. Ben-David, J. M. L. Martin, D. Milstein, *J. Am. Chem. Soc.* **1998**, *120*, 12539–12544.

[40] L. J. L. Häller, M. J. Page, S. A. Macgregor, M. F. Mahon, M. K. Whittlesey, *J. Am. Chem. Soc.* **2009**, *131*, 4604–4605.

[41] M. Albrecht, *Chem. Rev.* **2009**, *109-109*, 576–623.

[42] For examples of Rh^V complexes, see: J. L. McBee, J. Escalada, T. D. Tilley, *J. Am. Chem. Soc.* **2009**, *131*, 12703–12713, and references therein.

[43] B. A. Arndtsen, R. G. Bergman, *Science* **1995**, *270*, 1970–1973.

[44] D. L. Strout, S. Zaric, S. Niu, M. B. Hall, *J. Am. Chem. Soc.* **1996**, *118*, 6068–6069.

[45] B. K. Corkey, F. L. Taw, R. G. Bergman, M. Brookhart, *Polyhedron* **2004**, *23*, 2943–2954.

[46] F. L. Taw, H. Mellows, P. S. White, F. J. Hollander, R. G. Bergman, M. Brookhart, D. M. Heinekey, *J. Am. Chem. Soc.* **2002**, *124*, 5100–5108.

[47] T. M. Gilbert, R. G. Bergman, *J. Am. Chem. Soc.* **1985**, *107*, 3502–3507; D. M. Heinekey, A. S. Hinkle, J. D. Close, *J. Am. Chem. Soc.* **1996**, *118*, 5353–5361.

[48] J. J. H. Edema, A. Meetsma, F. Van Bolhuis, S. Gambarotta, *Inorg. Chem.* **2002**, *41*, 2056–2061.

[49] When the propyl substituent of the PH_2nPr ligand was replaced with hydrogen, the phosphane axial isomer ceased to be even a local minimum. The presence of the agostic interaction is, therefore, also important in stabilizing the observed geometry.

[50] See the Supporting Information for full details.

[51] R. B. Calvert, J. R. Shapley, *J. Am. Chem. Soc.* **1978**, *100*, 7726–7727; L. Mole, J. L. Spencer, N. Carr, A. G. Orpen, *Organometallics*

1991, *10*, 49–52; A. C. Albeniz, G. Schulte, R. H. Crabtree, *Organometallics* **1992**, *11*, 242–249; E. Clot, J. Y. Chen, D. H. Lee, S. Y. Sung, L. N. Appelhans, J. W. Faller, R. H. Crabtree, O. Eisenstein, *J. Am. Chem. Soc.* **2004**, *126*, 8795–8804; D. Buccella, G. Parkin, *J Am Chem. Soc* **2006**, *128*, 16358–16364; A. Toner, J. Matthes, S. Gruendemann, H. Limbach, B. Chaudret, E. Clot, S. Sabo-Etienne, *Proc. Natl. Acad. Sci. USA* **2007**, *104*, 6945–6950; A. B. Chaplin, A. I. Poblador-Bahamonde, H. A. Sparkes, J. A. K. Howard, S. A. Macgregor, A. S. Weller, *Chem. Commun.* **2009**, 244–246; T. Ishida, Y. Mizobe, M. Hidai, *Chem. Lett.* **1989**, 2077–2080.

[52] The small models **8'** and **9'** provided much lower barriers to C–H activation and also overestimated the stability of the intermediate formed upon alkyl deprotonation (see the Supporting Information).

[53] Alternative mechanisms included the formation of a Rh^V alkyl hydride species by oxidative addition and the transfer of the agostic proton onto the bromide ligand. In both cases the products formed were too high in energy for these processes to be feasible. In addition, attempts to effect the direct deprotonation of the agostic proton by external PMe_3 saw the system rearrange to the geminal deprotonation transition state.

[54] M.-D. Su, S.-Y. Chu, *J. Am. Chem. Soc.* **1997**, *119*, 5373–5383; A. J. Toner, S. Grundemann, E. Clot, H.-H. Limbach, B. Donnadieu, S. Sabo-Etienne, B. Chaudret, *J. Am. Chem. Soc.* **2000**, *122*, 6777–6778; Z. Y. Lin, *Coord. Chem. Rev.* **2007**, *251*, 2280–2291; W. H. Lam, G. C. Jia, Z. Y. Lin, C. P. Lau, O. Eisenstein, *Chem. Eur. J.* **2003**, *9*, 2775–2782.

[55] J. Oxgaard, R. P. Muller, W. A. Goddard, R. A. Periana, *J. Am. Chem. Soc.* **2003**, *125*, 352–363; N. A. Foley, M. Lail, T. B. Gunnoe, T. R. Cundari, P. D. Boyle, J. L. Petersen, *Organometallics* **2007**, *26*, 5507–5516.

[56] Calculations in the absence of PMe_3 gave a very similar energy barrier of 24.6 kcal mol^{-1}, confirming that external PMe_3 plays no role in the σ-bond metathesis process.

[57] A. B. Pangborn, M. A. Giardello, R. H. Grubbs, R. K. Rosen, F. J. Timmers, *Organometallics* **1996**, *15*, 1518–1520.

[58] W. E. Buschmann, J. S. Miller, K. Bowman-James, C. N. Miller, *Inorg. Synth.* **2002**, *33*, 83–85.

[59] A. T. Lubben, J. S. McIndoe, A. S. Weller, *Organometallics* **2008**, *27*, 3303–3306.

[60] A. M. Cosier, J. Glazer, *J. Appl. Crystallogr.* **1986**, *19*, 105.

[61] Z. Otwinowski, Z. Minor, *Methods Enzymol.* **1997**, 276.

[62] G. M. Sheldrick, *Acta Crystallogr. Sect. A* **2008**, *64*, 112–122.

[63] M. C. Burla, R. Caliandro, M. Camalli, B. Carrozzini, G. L. Cascarano, L. D. Caro, C. Giacovazzo, G. Polidori, R. Spagna, *J. Appl. Crystallogr.* **2005**, *38*, 381.

[64] P. W. Betteridge, J. R. Carruthers, R. I. Cooper, K. Prout, D. J. Watkin, *J. Appl. Crystallogr.* **2003**, *36*, 1487.

[65] Gaussian 03, Revision C.02, M. J. Frisch, G. W. Trucks, H. B. Schlegel, G. E. Scuseria, M. A. Robb, J. R. Cheeseman, J. A. Montgomery, Jr., T. Vreven, K. N. Kudin, J. C. Burant, J. M. Millam, S. S. Iyengar, J. Tomasi, V. Barone, B. Mennucci, M. Cossi, G. Scalmani, N. Rega, G. A. Petersson, H. Nakatsuji, M. Hada, M. Ehara, K. Toyota, R. Fukuda, J. Hasegawa, M. Ishida, T. Nakajima, Y. Honda, O. Kitao, H. Nakai, M. Klene, X. Li, J. E. Knox, H. P. Hratchian, J. B. Cross, V. Bakken, C. Adamo, J. Jaramillo, R. Gomperts, R. E. Stratmann, O. Yazyev, A. J. Austin, R. Cammi, C. Pomelli, J. W. Ochterski, P. Y. Ayala, K. Morokuma, G. A. Voth, P. Salvador, J. J. Dannenberg, V. G. Zakrzewski, S. Dapprich, A. D. Daniels, M. C. Strain, O. Farkas, D. K. Malick, A. D. Rabuck, K. Raghavachari, J. B. Foresman, J. V. Ortiz, Q. Cui, A. G. Baboul, S. Clifford, J. Cioslowski, B. B. Stefanov, G. Liu, A. Liashenko, P. Piskorz, I. Komaromi, R. L. Martin, D. J. Fox, T. Keith, M. A. Al-Laham, C. Y. Peng, A. Nanayakkara, M. Challacombe, P. M. W. Gill, B. Johnson, W. Chen, M. W. Wong, C. Gonzalez, J. A. Pople, Gaussian, Inc., Wallingford CT, **2004**.

[66] D. Andrae, U. Haussermann, M. Dolg, H. Stoll, H. Preuss, *Theor. Chim. Acta.* **1990**, *77*, 123–141.

[67] A. Höllwarth, M. Böhme, S. Dapprich, A. W. Ehlers, A. Gobbi, V. Jonas, K. F. Köhler, R. Stegmann, A. Veldkamp, G. Frenking, *Chem. Phys. Lett.* **1993**, *208*, 237–240.

[68] P. Hariharan, J. A. Pople, *Theor. Chim. Acta.* **1973**, *28*, 213–222; W. J. Hehre, R Ditchfie, J. A. Pople, *J. Chem. Phys.* **1972**, *56*, 2257–2261.

Received: March 3, 2010
Published online: June 22, 2010

